High-Field Electron $g-2$ Measurement*

John C. Wesley† and Arthur Rich
The Harrison M. Randall Laboratory of Physics, The University of Michigan, Ann Arbor, Michigan 48104
(Received 9 April 1971)

We have measured the g-factor anomaly of the free electron to an accuracy of ±3 ppm (68% confidence level). The method (a refinement of that used by Wilkinson and Crane in 1963) is based on a direct observation of the difference between the spin precession and cyclotron frequencies of 100-keV electrons confined in a precisely measured magnetic mirror trap. An order of magnitude increase in precision over the Wilkinson-Crane experiment has been achieved by (a) a tenfold increase in the magnitude of the magnetic field (to 1 kG), and (b) a tenfold reduction in the relative depth of the magnetic trap (to 60 ppm). An extensive series of tests for systematic effects at the 1-ppm level has also been carried out. With $a=\frac{1}{2}(g-2)$, we find $a_{\text{expt}}(e^-)=(1\,159\,657.7\pm3.5)\times10^{-9}$. The difference between this result and the current theoretical expression for a, as calculated through second order in the fine-structure constant α, is $a_{\text{expt}}(e^-)-[0.5\,(\alpha/\pi)-0.328\,48\,(\alpha/\pi)^2]=(1.68\pm0.33)\,(\alpha/\pi)^3$. In the above, we have used $\alpha^{-1}=137.036\,08\pm0.000\,26$, as recently recommended by Taylor, Parker, and Langenberg. The uncertainty in the coefficient is the rms sum of our experimental error and the uncertainty in α^{-1}. In this form, our result can be interpreted as an experimental determination of the sixth-order quantum-electrodynamic contribution to the anomaly. Current estimates of this quantity are $1.49\,(\alpha/\pi)^3$.

I. INTRODUCTION

A. Electron g Factor and Quantum Electrodynamics

Although precision measurements of the electron g factor[1] play an important role in metrology and least-squares adjustments of the fundamental constants,[2] their primary importance has been as a means of testing the predictions of quantum electrodynamics (QED). The g-factor anomaly $a\,(a\equiv\frac{1}{2}(g-2))$ is due entirely to quantum-electrodynamic effects. It is most naturally expressed as a power-series expansion in the fine-structure constant α $(\alpha=e^2/\hbar c\cong1/137)$; i.e.,

$$a=A\,(\alpha/\pi)+B\,(\alpha/\pi)^2+C\,(\alpha/\pi)^3+\cdots\,. \tag{1}$$

Since the terms of this expansion involve successive powers of e^2, the coefficients A, B, and C are referred to as the second-, fourth-, and sixth-order coefficients. Each coefficient can be evaluated by using the "rules" of QED to convert appropriate Feynman diagrams to equivalent integral expressions.[3] Evaluation of the integrals leads to a numerical result for the coefficient. An exact solution has been possible in second and fourth orders. Schwinger[4] has obtained the result $A=\frac{1}{2}$, while Petermann[5] and Sommerfield[6] have obtained[7]

$$B=\tfrac{197}{144}+\tfrac{1}{12}\pi^2+\tfrac{3}{4}\zeta(3)-\tfrac{1}{2}\pi^2\ln2=-0.328\,48\ldots$$

(ζ is the Riemann ζ function).

At the present time no complete calculation of C is available. Drell and Pagels[8] and Parsons[9] have used dispersion theory to estimate C as 0.13. Various sixth-order diagrams containing electron loops (vacuum polarization) have been explicitly calculated by Mignaco and Remiddi,[10] Aldins et al.,[11] and Brodsky and Kinoshita.[12] The combined contribution of all sixth-order diagrams involving electron loops is $(0.26\pm0.05)(\alpha/\pi)^3$ (the uncertainty is due to error in numerical integration). Brodsky and Kinoshita[12] have suggested that the dispersion-theory estimate does not include these diagrams. Accordingly, they propose that the contribution of the electron-loop diagrams be combined with the dispersion-theory estimate, to give $C=0.39$. We note that Levine and Wright[13] have found the combined contribution of three additional sixth-order diagrams to be $-1.79\times(\alpha/\pi)^3$. It is, of course, possible that other diagrams will cancel this large negative contribution.

It is clear from the above that any speculation on the theoretical value of the sixth-order coefficient is premature. There are currently (to our knowledge) six groups independently working on the evaluation of C. Hopefully, definitive results will be forthcoming in the near future, at which time it will be possible to compare theory and experiment to order α^3. We note here that when our experimental result for a is expressed as a power series in α with A and B as quoted above, we find $C=1.68\pm0.33$ (see Sec. V for the details of this reduction).

Note added in proof. Levine and Wright[13a] have recently completed the theoretical calculation of C. Their result is $C=1.49\,(\alpha/\pi)^3$, in excellent agreement with our experimental value.

B. Motivation for Present Experiment

In order to clarify the motivation for our present work, we will briefly review recent events related to the comparison of experimental measurements and theoretical estimates of the electron anomaly. In 1963, Wilkinson and Crane[14] found $a_{\text{expt}}^{\text{WC}}$ (1963) $= (1\,159\,622 \pm 27) \times 10^{-9}$, in excellent agreement with the then current theoretical estimate a_{theor} (1963) $= (1\,159\,615 \pm 12) \times 10^{-9}$, as obtained by evaluating Eq. (1) using $A = \frac{1}{2}$, $B = -0.328\,48$, $C = 0 \pm 1$, and $\alpha^{-1} = 137.039\,1 \pm 0.0006$. This value of α was obtained using QED to interpret measurements of the fine-structure intervals of deuterium.[15]

By 1968, a series of events had transformed the 1963 agreement between theory and experiment into a 3-standard-deviation discrepancy. In 1968 Rich[16] and Farley[17] recognized that several systematic errors were present in the original result of Wilkinson and Crane. After applying corrections to the original data, the revised experimental result was[16] $a = (1\,159\,557 \pm 30) \times 10^{-9}$. In 1969, Henry and Silver[18] noted the necessity for an additional correction that further reduced the result to $a_{\text{expt}}^{\text{WC}}$ (1969) $= (1\,159\,549 \pm 30) \times 10^{-9}$. Also by 1969, the theoretical value of the anomaly had increased to a_{theor} (1969) $= (1\,159\,637 \pm 11) \times 10^{-9}$, owing entirely to the use of the revised value $\alpha_{\text{WQED}}^{-1} = 137.036\,08 \pm 0.000\,26$, as obtained without recourse to QED theory.[2]

A measurement of a to ± 3 ppm would not only serve to unambiguously check the revised Wilkinson-Crane result, but could also be interpreted as a test of QED to sixth order, assuming that C is of order unity [note that $(\alpha/\pi)^3 = 11$ ppm of α]. Alternatively, if the validity of QED and Eq. (1) is accepted, such a measurement could be interpreted as providing a determination of α to ± 3 ppm.

C. Experimental Method

Our present experiment (hereafter g-IV) is essentially an improved version of the experiment of Wilkinson and Crane[14] (hereafter g-III). The technique involves a direct observation of the difference between the cyclotron and spin precession frequencies of electrons trapped in a known magnetic field. Mott scattering is used both to initially polarize the electrons and to detect their final spin orientation.

The entire experiment takes place in a 1-kG magnetic field (Fig. 1). A 100-nsec pulse of unpolarized 100-keV electrons is scattered from a gold foil target. Those electrons which scatter elastically in a direction nearly perpendicular to the magnetic field are partially polarized, with polarization P normal to both their velocity $\vec{v}$ and the field direction. The scattered electrons drift in a helix of 1.0-cm radius and 0.1-cm pitch into the trapping region. The field is shaped to form a magnetic mirror trap, with the field intensity at either end approximately 60 ppm stronger than at the center. The trapping region is enclosed by a pair of metal cylinders (Fig. 1). A 100-nsec positive voltage pulse is applied to the injection cylinder as the scattered electrons drift across the gap between the cylinders. Consequently, the electrons lose sufficient axial velocity so that they became permanently trapped by the magnetic field.

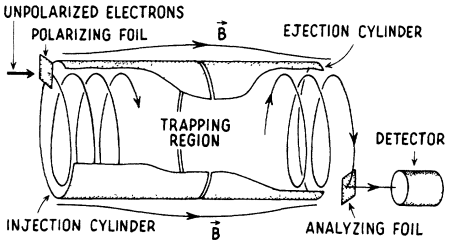

FIG. 1. Experimental method (schematic).

The electrons are held in the trap for an accurately determined time T. A positive pulse on the ejection cylinder then gives them sufficient axial velocity to reach a second gold foil target, which is used to analyze their final spin orientation. Those electrons which scatter through 90° are counted.

While the electrons are in the magnetic field, their velocity $\vec{v}$ and polarization $\vec{P}$ precess at frequencies ω_c and ω_S, respectively. The relative precession of $\vec{P}$ with respect to $\vec{v}$ occurs at the beat or difference frequency between ω_S and ω_c. If $\vec{v}$ is perpendicular to a uniform magnetic field $\vec{B}$, the difference frequency $\omega_D \equiv \omega_S - \omega_c$ has the simple form

$$\omega_D = a\gamma\omega_c = a\omega_0 , \tag{2}$$

where $\omega_0 = eB/m_0c$, $\gamma = (1 - v^2/c^2)^{-1/2}$, and $\omega_c = \omega_0/\gamma$.

The ejection process is arranged so that the arrival direction of electrons incident on the analyzing foil is independent of T. Because of the Mott scattering asymmetry, the fraction of the electrons scattered into the detector varies as $\vec{P} \cdot \vec{v}$. If the number of electrons ejected from the trap is independent of T, the counting rate at the detector will be

$$R(T) = R_0\{1 + \delta \cos(\omega_D T + \phi)\} , \tag{3}$$

where R_0 is the rate for unpolarized electrons, δ is the Mott asymmetry factor (typically 0.02), and ϕ is a phase constant. The difference frequency is determined by sampling $R(T)$ at various values of T and fitting the data by least squares to obtain the position of two maxima of $R(T)$. If N oscillations of $R(T)$ are observed between $T = T_1$ and $T = T_2$, then $\omega_D = 2\pi N/(T_2 - T_1)$.

The zero-energy cyclotron frequency ω_0 is deter-

mined indirectly by measuring the magnetic field in terms of the resonance frequency $\omega_p(H_2O)$ of protons in water. The conversion to ω_0 is accomplished using the relation

$$\omega_0 = (\mu_p'/\mu_B)^{-1}\ \omega_p(H_2O)\ , \tag{4}$$

where μ_p'/μ_B is the proton magnetic moment in Bohr magnetons ($\mu_B = e\hbar/2m_0c$), measured with protons in a water sample. The anomaly is then simply the ratio ω_D/ω_0.

D. Improvements in g-IV

Equation (2) is exact only for planar cyclotron motion perpendicular to a uniform magnetic field. As we will show in Sec. II B, it is necessary to add correction terms to Eq. (2) to account accurately for the orbital motion and fields encountered in the trapping region. The primary goal in the design of g-IV was to minimize the magnitude of these corrections. Major innovations with respect to g-III are a tenfold increase of the magnetic field (to 1 kG), a tenfold decrease in the relative depth of the trap (to 60 ppm), and an explicit measurement of the distribution of the axial momentum of the trapped electrons. These innovations (i) permit the use of up to 2×10^4 cycles of $R(T)$ in the determination of ω_D, thus reducing the statistical uncertainty in ω_D to less than ± 1 ppm, (ii) reduce the uncertainty in evaluating the average magnetic field experienced by the trapped electrons to ± 1 ppm, and (iii) reduce the systematic shift in ω_D due to stray electric fields to less than 5 ppm. In g-IV, the largest correction to Eq. (2) is approximately 10 ppm, an order of magnitude smaller than the corrections in g-III. We have also made an extensive series of tests for a systematic dependence of ω_D on various experimental parameters. On the basis of these tests, we estimate that the systematic error in our final result is less than ± 1 ppm of a.

II. THEORY

A. Orbital Motion of Trapped Electrons

The orbital motion of the electrons in the magnetic trap is most easily obtained through the use of the adiabatic invariance of the magnetic moment of the electron orbit μ_{orb}.[19] Consider the motion of an electron in a magnetic field $\vec{B}(r,z)$ which is predominantly in the z direction, and which varies slightly as a function of the axial coordinate z. Let the electron velocity $\vec{v}$ have components $v_\perp$ and v_z normal and parallel to the z axis, let the orbit center coincide with the z axis, and let the cyclotron radius be r_c. For these conditions μ_{orb} [defined as $c^{-1}(e\omega_c/2\pi)\pi r_c^2$] is given by the expression $\frac{1}{2}\gamma m_0 v_\perp^2/|\vec{B}(r_c,z)|$. If the variation of $\vec{B}$ is sufficiently small over both r_c and the pitch of the helical trajectory, μ_{orb} becomes an adiabatic invariant. For the g-IV magnetic trap, the fractional variation in μ_{orb} is of order 0.1% of the fractional variation in $\vec{B}$ over the trapping region.[20,21] In the material that follows, we will explicitly use the axial velocity to evaluate corrections of order 10% of the fractional variation in $\vec{B}$. For this purpose, μ_{orb} can be treated as a rigorous constant of the motion. Since no significant electric fields are present, $|\vec{v}|$ is also treated as a constant.

Consider the motion of an electron in the magnetic field shown in Fig. 2, where $B(z) = |\vec{B}(r_c,z)|$. Let the electron have $v_z(z_1) = 0$. The relation $v^2 = v_\perp^2 + v_z^2$, together with the invariance of μ_{orb} and v leads to

$$v_z(z) = v\left(\frac{B(z_1)-B(z)}{B(z_1)}\right)^{1/2}. \tag{5a}$$

We have used the approximations $v_\perp(z) = v$, and $B(z) = B(z_1)$, each of which holds to better than 1 part in 10^4 in the g-IV trap. The left-hand turning point of the axial motion (z_2) is determined by the condition $B(z_2) = B(z_1)$.

If the square of Eq. (5a) is multiplied by $\frac{1}{2}\gamma m_0$, the result

$$\tfrac{1}{2}\gamma m_0 v_z^2(z) = \tfrac{1}{2}\gamma m_0 v^2\{B(z_1)-B(z)\}/B(z_1) \tag{5b}$$

can be interpreted as an equation of axial motion for an electron with an effective "axial kinetic energy" $T_z(z) = \frac{1}{2}\gamma m_0 v_z^2(z)$ moving in an effective "axial potential" given by

$$U(z) = -\tfrac{1}{2}\gamma m_0 v^2\{B(z_1)-B(z)\}/B(z_1)\ . \tag{6}$$

To within the approximations used above, $U(z)$ is the work done by the axial component of the magnetic force on the electron, as the electron moves from z_1 to z [see Sec. II C, Eq. (13a) for a further interpretation of this point].

The period τ for a complete axial oscillation of

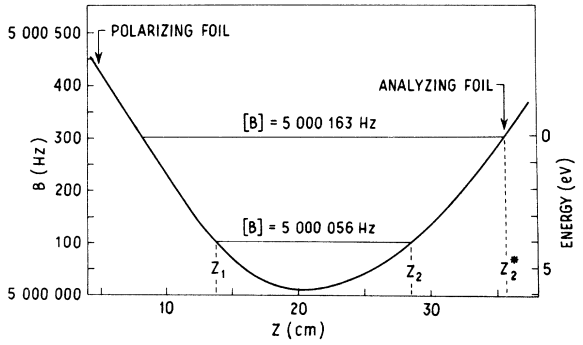

FIG. 2. Magnetic field in the trapping region. The field is measured in terms of proton resonance frequency (left-hand scale). The energy scale on the right gives the equivalent potential for axial motion. The time-average field is shown for the levels $B' = B_{max}$ and $B' = B_{min}$ (see Sec. II C).

an electron can be calculated from the dependence of $B(z)$ on z. Using $dt = dz/v_z$ and integrating over complete oscillation leads to

$$\tau(z_1) = \int_{z_1}^{z_2} \frac{dz}{v_z(z)} + \int_{z_2}^{z_1} \frac{dz}{v_z(z)}$$

$$= \frac{2B(z_1)^{1/2}}{v} \int_{z_1}^{z_2} \frac{dz}{\{B(z_1) - B(z)\}^{1/2}} \quad . \qquad (7)$$

For the well shown in Fig. 2 and an electron energy of 110 keV, the period is approximately 600 nsec, corresponding to a 1.5-MHz axial oscillation frequency. The cyclotron frequency is approximately 4000 MHz. Within the trapping region, the maximum value of $\{B(z_1) - B(z)\}/B(z_1)$ is 60×10^{-6}. The equivalent potential well for axial motion is therefore about 6-eV deep.

The axial oscillation frequency was measured by applying a small ($\cong$ 0.1-V rms) continuous sinusoidal rf voltage between the trapping cylinders. Resonance between the applied rf and the oscillating electrons permits the electrons to gain sufficient axial energy to remove them from the trap before the normal ejection pulse. Consequently, at resonance, the counting rate decreases sharply. The resonance frequency determined in this manner was compared to the predicted frequency obtained by numerical integration of Eq. (7) from field-map data (Sec. IV B). The frequencies agreed to 1%, thus providing a convincing check of the orbit theory developed above.

Orbit Perturbations

If the orbit center does not coincide with the field center, an additional perturbation of the orbit is present, which causes the orbit center to drift slowly about the field center on a circular trajectory. For the g-IV trap, the period of this so-called Ω motion is approximately 3000 μsec.[21] The only observable effect of the Ω motion is an extremely slow periodic variation of beam intensity with trapping time. Since the period of the motion is much greater than the difference frequency period, this variation has no significant effect on the asymmetry function of Eq. (3).

Small departures of the magnetic field from circular symmetry also give rise to a drift of the orbital center. If a weak external field gradient of the form $\partial B_z/\partial x$ is superimposed on an initially symmetric field, the orbit center of the trapped electrons will begin to drift perpendicularly to both the external field gradient and the z axis. The orbit center will not, however, drift monotonically away from the z axis, but instead will eventually be returned to the vicinity of the z axis on an approximately circular trajectory.[21] The necessary restoring force on the electron arises from the radial field gradient ($\partial B_z/\partial r$) associated with the trap. This gradient increases in proportion to r, and so will eventually predominate over any external gradient. The radius of the drift trajectory increases as the magnitude of the external gradient is increased. If the external gradient is large enough, the electrons will drift far enough from the mechanical axis of the apparatus (the z axis) to strike the walls of the trapping cylinders. In order to prevent this, the magnetic field must be made highly symmetric about the mechanical axis of the apparatus. This is accomplished by introducing an external field gradient that is adjustable in magnitude and direction to cancel the residual asymmetry in the main solenoid field. Improper adjustment of the magnitude of the external gradient by 0.2 ppm/cm is sufficient to reduce the beam intensity by a factor of 2. The use of external gradient compensation is essential to trapping in the weak g-IV trap.

Both qualitative and quantitative aspects of the Ω motion and gradient drift can be predicted using a simple theory relating the instantaneous drift velocity of the orbit center to the average field gradient over the electron orbit.[21] We find good agreement between the predicted and observed values of the Ω period and the sensitivity of the beam intensity to the uncompensated field gradient,[21] thus indicating a satisfactory understanding of the long-term motion of the trapped electrons.

B. Spin Motion of Trapped Electrons

The exact classical[22] equations of motion for an electron with spin $\vec{S}$, magnetic moment $\frac{1}{2}g(e/m_0c)\vec{S}$, and velocity $\vec{v}$ in fields $\vec{B}(\vec{r})$ and $\vec{E}(\vec{r})$ can be put into the form[23]

$$\frac{d\hat{v}}{dt} = \vec{\Omega}_v \times \hat{v} \, , \qquad (8a)$$

$$\frac{d\vec{S}}{dt} = \vec{\Omega}_S \times \vec{S}, \qquad (8b)$$

where

$$\vec{\Omega}_v = -\frac{e}{m_0 c}\left(\frac{\vec{B}}{\gamma} - \frac{\gamma}{\gamma^2 - 1}\,\vec{\beta}\times\vec{E}\right) \, ,$$

$$\vec{\Omega}_S = -\frac{e}{m_0 c}\left\{\frac{\vec{B}}{\gamma} - \frac{\gamma}{\gamma+1}\,\vec{\beta}\times\vec{E} + a\left(\vec{B} - \frac{\gamma\vec{\beta}}{\gamma+1}\,\vec{\beta}\cdot\vec{B} - \vec{\beta}\times\vec{E}\right)\right\} \, ,$$

and $\vec{\beta} = \vec{v}/c$. To obtain an explicit solution for $\vec{S}(t)$, it is necessary to integrate these equations together with $d\vec{r}/dt = \vec{v}$. The observable quantity is $\vec{S}(t)\cdot\hat{n}$, where $\hat{n} = (\hat{v}\times\hat{v}')/|\hat{v}\times\hat{v}'|$, $\hat{v}$ and $\hat{v}'$ being the directions of electron motion before and after the second Mott scattering.

In practice, such an exact solution is not possible except for the case of motion in a spatially uniform magnetic field. In this case, $\vec{S}\cdot\hat{n}$ oscillates with frequency

$$\omega_D = |\vec{\Omega}_D| = a\omega_0/\gamma_z , \tag{9}$$

where $\vec{\Omega}_D = \vec{\Omega}_S - \vec{\Omega}_v$, $\gamma_z = (1 - v_z^2/c^2)^{-1/2}$, v_z is the axial component of $\vec{v}$, and $\vec{B}$ is in the axial (z) direction.[18,23]

For general fields $\vec{E}$ and $\vec{B}$, $\vec{\Omega}_D$ has the form

$$\vec{\Omega}_D = -\frac{e}{m_0 c}\left\{a\vec{B} - a\frac{\gamma}{\gamma+1}(\vec{\beta}\cdot\vec{B})\vec{\beta} + \left(\frac{1}{\beta^2\gamma^2} - a\right)\vec{\beta}\times\vec{E}\right\} . \tag{10}$$

The equation of motion for $\vec{S}$ in a frame rotating with $\vec{v}$ is $d\vec{S}/dt = \vec{\Omega}_D\times\vec{S}$. The instantaneous motion of $\vec{S}$ is a precession about $\vec{\Omega}_D$ with angular velocity $\omega_D = |\vec{\Omega}_D|$. However, $\vec{\Omega}_D$ is no longer parallel to the z axis, but has a component $\Omega_{D\perp}$ normal to z which rotates at $|\vec{\Omega}_v|$. The magnitudes of both Ω_{Dz} and $\Omega_{D\perp}$ also vary as a function of the instantaneous values of $\vec{E}$, $\vec{B}$, and $\vec{\beta}$.

Although an explicit solution is not feasible, it is possible to obtain a satisfactory approximation to the average motion of $\vec{S}$ over a complete axial oscillation in the trap. We note that for the parameters of g-IV (i) the axial oscillation frequency is less than $10^{-3}\omega_c$, and (ii) the maximum value of $\Omega_{Dz}/\Omega_{D\perp}$ is about 10^{-3}, and therefore the angle that $\vec{\Omega}_D$ makes with the z axis is correspondingly small. If one averages over the cyclotron motion, the remaining rates of variation of the parameters of the equation of motion will be sufficiently small that *the average motion of* $\vec{S}$ *with respect to* $\vec{v}$ *over a complete axial oscillation will be a precession about the z axis with an average frequency* $[\omega_D] = [|\vec{\Omega}_D|]$.[24] The notation $[\ ]$ indicates that the enclosed quantity is to be time averaged over a complete axial oscillation. Since electrons are always observed after a half-integral number of axial oscillations, the time-averaged quantities are the only experimentally observable ones. So long as the axial and difference frequencies are not equal, the true motion of $\vec{S}$ deviates from a uniform precession at frequency $[\omega_D]$ by an angle of order $\Omega_{Dz}/\Omega_{D\perp}$, corresponding to a slight "wobble" superimposed on the otherwise uniform motion. Neglecting the effects of this wobble will result in a phase error of the order of $2\pi\times10^{-3}$. Since the total phase difference between inner and outer trapping time is $2\pi N$, and since N is typically about 10^4, the relative error in a due to approximating the true motion of $\vec{S}$ by a uniform precession is of order 0.1 ppm.

If the axial and difference frequencies are nearly equal, the above analysis breaks down. At resonance, a secular rotation of $\vec{S}$ out of the plane normal to $\hat{z}$ can occur; this rotation would be observed as an apparent depolarization of the trapped beam. We have found no experimental evidence for such a resonant depolarization. Because of the small value of $\Omega_{Dz}/\Omega_{D\perp}$, we expect that the width of any possible resonances will be extremely small.[25]

To interpret the data in g-IV, we will therefore assume that $\vec{S}\cdot\hat{n}$ will oscillate at a frequency $[\omega_D] = [|\vec{\Omega}_D|]$. This assumption is the basis of Eq. (11) below and for the final determination of a. We believe that the error introduced in using this assumption is negligible in comparison with other errors present. Ford and Granger[26] are attempting to check both the validity of the above assumption and the effect of possible resonances by integrating Eqs. (8a) and (8b) by perturbation methods.

By explicitly introducing the magnitudes of the magnetic and electric fields encountered in the trapping region, it is possible to obtain a simplified expression for $[\omega_D]$. For time-average electric fields less than 1 V/cm (our observed fields are less than 3 mV/cm), the following expansion is accurate[21] to 0.1 ppm of a:

$$\frac{[\omega_D]}{[\omega_0]} = a - \frac{a}{2}[\beta_z^2] - \frac{1}{\beta\gamma^2}\frac{[E_\perp]}{[B_z]} + \frac{1}{2a}\left(\frac{1}{\beta\gamma^2}\right)^2\frac{[E_z^2]}{[B_z^2]} , \tag{11}$$

where $E_\perp$ and E_z are components of $\vec{E}$ normal and parallel to $\hat{z}$. A comparison of this result with Eq. (9) shows that the first two terms of Eq. (11) correspond to the time-averaged expansion of Eq. (9) using $\gamma_z = 1 + \frac{1}{2}\beta_z^2 + \cdots$. An equation similar to Eq. (11) was derived and used in g-III. That equation contained a term $\{\gamma/(\gamma+1)\}[\beta_z^2]$. The factor $\gamma/(\gamma+1)$ is obtained if one time averages *before* rather than *after* taking the absolute value of $\vec{\Omega}_D$. Replacement of the factor of $\gamma/(\gamma+1)$ by a factor of $\frac{1}{2}$ was responsible for the further reduction of the revised g-III value for a from $1\,159\,557\times10^{-9}$ to $1\,159\,549\times10^{-9}$, as cited in Sec. I B. The proper axial velocity correction term was first obtained by Henry and Silver.[18] They were able to derive Eq. (9) from Eq. (2) by noting that helical motion of an electron with axial velocity v_z is equivalent to viewing planar cyclotron motion from a reference frame drifting parallel to $\hat{z}$ with velocity $-v_z$. In the drifting frame, the observed value of ω_D is simply $a\omega_0/\gamma_z$. As noted above, this result is also implicit in the formulations of Ref. 23, when the quantity that is being measured is properly identified as $[|\vec{\Omega}_D|]$, rather than $|[\vec{\Omega}_D]|$.

For $[E_z^2] = 10^4\ \mathrm{mV^2/cm^2}$, the quadratic term in Eq. (11) is about 0.2 ppm of a. Since our final data show no evidence of a quadratic dependence of $[\omega_D]/[\omega_0]$, and since we have additional justification[21] for believing $[E_z^2]$ to be considerably less than $10^4\ \mathrm{mV^2/cm^2}$, we will drop the quadratic term of Eq. (11) in what follows.

The time-averaged quantities will depend on the amplitude of oscillation of the electron in the well, so an additional average over the ensemble of

trapped electrons is necessary. This ensemble average will be indicated by the notation $\langle\ \rangle$. The ensemble average of Eq. (11) becomes, after a slight rearrangement,

$$a' = a - \langle[E_\perp]\rangle X = \frac{\langle[\omega_D]\rangle}{\langle[\omega_0]\rangle}\left(1+\frac{\langle[\beta_z^2]\rangle}{2}\right) , \qquad (12)$$

where $X = (\beta\gamma^2 B)^{-1} \cong (\beta\gamma^2\langle[B_z]\rangle)^{-1}$. All quantities on the right-hand side of Eq. (12) can be determined experimentally. The quantity $\langle[\omega_D]\rangle$ is the frequency obtained from the trapping time interval between maxima of the asymmetry curve. The quantities $\langle[\omega_0]\rangle$ and $\langle[\beta_z^2]\rangle$ may be evaluated from measurements of the magnetic field and the amplitude distribution of the trapped electrons. There is no direct way to measure or calculate $\langle[E_\perp]\rangle$. If $\langle[E_\perp]\rangle$ is independent of X and constant in time, a can be obtained by measuring a' as a function of X and extrapolating to $X = 0$ ($B \to \infty$). In g-IV, a' is measured at four values of B, corresponding to $X = 1.02$, 1.31, 1.69, and 2.28 kG^{-1}. The electron energy is varied from 108 to 56 keV in such a manner as to maintain a 1.0-cm cyclotron radius at each magnetic field.

C. Time and Ensemble Averages

In order to evaluate the ensemble averages, it is necessary to determine the axial amplitude distribution of the trapped electrons. It will be convenient to characterize this distribution in terms of the number of electrons oscillating at a level B', where $B' = B(z_1) = B(z_2)$. The maximum amplitude of oscillation is determined by the location of the analyzing foil at $z = z_2^*$ (Fig. 2). The maximum level in the trap is therefore $B_{\max} = B(z_2^*)$. Electrons at a level B' have a total axial energy

$$\Delta U(B(z_2^*), B') = -\tfrac{1}{2}\gamma m_0 v^2 \{B(z_2^*) - B'\}/B(z_2^*) \qquad (13a)$$

relative to electrons at the level $B(z_2^*)$. If a voltage V is applied to the ejection cylinder, only electrons above the level $\Delta U = -eV$ will acquire sufficient axial energy to reach the analyzing foil. If the number of electrons ejected by V is $N(V)$, the relative density of electrons at the level $\Delta U = -eV$ is $\rho(\Delta U) = dN(V)/dV$. The conversion from ejection voltage to depth below the level of the analyzing foil is

$$\Delta B/\Delta V = eB(z_2^*)/\tfrac{1}{2}\gamma m_0 v^2 , \qquad (13b)$$

where $\Delta B = B(z_2) - B'$. In the actual data runs, the ejection voltage used (V^*) ejects electrons from approximately the upper two-thirds of the well. The minimum useful well level is therefore $B_{\min} = B(z_2^*) - (\Delta B/\Delta V)V^*$ (Fig. 2). The number of electrons at each level of the well is given by a density function $\rho(B') = k\rho(\Delta U)$, where the conversion constant k includes a normalization factor such that

$$\int_{B_{\min}}^{B_{\max}} \rho(B')dB' = 1 .$$

The time-average field of an electron at the level B' is

$$[B(B')] = \frac{2}{\tau(z_1)}\int_{z_1}^{z_2}\frac{B(z)}{v_z(z)}\,dz$$

$$= B(z_1) - \frac{\int_{z_1}^{z_2}\{B(z_1) - B(z)\}^{1/2}dz}{\int_{z_1}^{z_2}\{B(z_1) - B(z)\}^{-1/2}dz} . \qquad (14)$$

Similarly, the time average of $\beta^2{}_z$ is

$$[\beta_z^2(B')] = \frac{2}{\tau(z_1)}\int_{z_1}^{z_2}\frac{\beta(z)}{v_z(z)}\,dz$$

$$= \frac{\beta^2}{B(z_1)}\,\frac{\int_{z_1}^{z_2}\{B(z_1) - B(z)\}^{1/2}dz}{\int_{z_1}^{z_2}\{B(z_1) - B(z)\}^{-1/2}dz} . \qquad (15)$$

The ensemble averages of these quantities are

$$\langle[B]\rangle = \int_{B_{\min}}^{B_{\max}}\rho(B')[B(B')]dB' \qquad (16)$$

and

$$\langle[\beta_z^2]\rangle = \int_{B_{\min}}^{B_{\max}}\rho(B')[\beta_z^2(B')]dB' . \qquad (17)$$

D. Asymmetry Data

In g-IV, recording of the asymmetry curve of Eq. (3) is complicated by the similarity of the difference frequency period τ_D (250 nsec) and the well oscillation period τ (600 nsec). Approximately one-half a well period is required to eject the electrons from the trap. Electrons will arrive at the analyzing foil (and the detector) at an approximately constant rate during the interval $\frac{1}{8}\tau \le t \le \frac{5}{8}\tau$, where t is the time of arrival with respect to the ejection pulse at $T = T_e$ (the additional delay of $\frac{1}{8}\tau$ is due to the transit time between the cylinder gap and the analyzing foil). The total time spent in the magnetic field is $T = T_e + t$, and the instantaneous counting rate at the detector will be

$$R(T) = R_0(T_e + t)\{1 + \delta\cos[\omega_D(T_e + t) + \phi]\} .$$

If all electrons are counted with a single scaler (as in g-III) the average counting rate will be

$$\int_{t=0}^{t=t_1} R(T_e + t)\,dt ,$$

where $t_1 \cong \frac{5}{8}\tau$. Since in g-IV $\tau_D \cong \frac{1}{2}\tau$, the integrated counting rate will show a greatly diminished asymmetry, since one is integrating the cosine function of Eq. (3) over an interval of approximately 2π. The full asymmetry will be obtained only if the counting rate is sampled over an interval small compared to τ_D. In order to use all the ejected electrons, the counting rate is sampled in a series of successive intervals of 33.3 nsec each, with the first interval beginning at $T = T_e$. The counting rate

in the Kth interval is therefore

$$R^K(T)=R_0^K\{1+\delta_K\cos[\omega_D[T_e+(K-1)(33.3\ \text{nsec})]+\phi_K]\}\},\quad(18)$$

where $K=1, 2, \ldots$. The parameters R_0^K, δ_K, and ϕ_K are to be determined from a least-squares fit of the data of $R^K(T)$ vs T. This results in K separate curves, which must be added numerically to obtain a single curve $R(T)$. Writing this out explicitly gives

$$R_0\{1+\delta\cos(\omega_D T+\phi)\}=\sum_K R_0^K\{1+\delta_K\cos(\omega_D T+\phi_K)\},$$

which can be solved to yield

$$R_0=\sum_K R_0^K,\quad(19a)$$

$$\delta=(F^2+G^2)^{1/2}/R_0,\quad(19b)$$

$$\phi=\tan^{-1}(F/G),\quad(19c)$$

where $F=\sum_K R_0^K\delta_K\sin\phi_K$, and $G=\sum_K R_0^K\delta_K\cos\phi_K$.

The parameters R_0, δ, and ϕ are the same as those which would be obtained if all electrons in the trap could be ejected and counted in a time short compared to τ_D. In effect, the summation that was automatically accomplished by using a single scaler in g-III is now performed (of necessity) numerically in g-IV.

E. Conversion from Proton to Electron Resonance Frequency

The magnetic field is measured in terms of the resonance frequency $\omega_p(M)$ of the NMR mapping probe (Sec. III B). The conversion to ω_0 is accomplished using the relation

$$\omega_0=\left(\frac{\omega_p(S)}{\omega_0}\right)^{-1}\frac{\omega_p(S)}{\omega_p(M)}\,\omega_p(M),\quad(20)$$

where $\omega_p(S)$ is the resonance frequency of a standard NMR probe (described below). The ratio $\omega_p(S)/\omega_0$ has been measured by Klein[27] to be

$$\omega_p(S)/\omega_0=(1.520\,994\,5\pm0.000\,000\,7)\times10^{-3}.\quad(21)$$

The ratio $\omega_p(S)/\omega_p(M)$ is a calibration factor obtained by comparing the resonance frequencies of the standard and mapper probes in the same magnetic field. Because the mapper probe must be small enough to fit within the trapping region, it is not possible to construct it in the standard probe configuration. Accordingly, it is expected that $\omega_p(S)/\omega_p(M)$ will differ from unity by up to several ppm, owing to the different bulk diamagnetic corrections associated with the different sample geometries and owing to possible nonzero susceptibility of the materials used to fabricate the mapper probe.

We have chosen to use Eq. (21), rather than alternate values of $\mu_p'/\mu B$,[28] because of the ease and accuracy with which Klein's standard probe can be reproduced and used. This probe consists of a long ($L/D\geq10$) cylindrical sample of 0.2M $CuSO_4$ solution, with the axis of the cylinder oriented normal to the magnetic field direction. This configuration has the important advantage that any possible uniform nonzero susceptibility of the materials used to fabricate the probe will have no appreciable effect on the magnetic field experienced by the proton sample. If an infinitely long hollow cylinder of permeability μ is placed in an initially uniform magnetic field with the cylinder axis normal to the field, the field inside the cylinder will be altered by a factor of order[27] $(\mu-1)^2$. For most "nonmagnetic" materials, $|\mu-1|\leq10^{-5}$, so the effect of such a cylinder is completely negligible at a level of 1 ppm [end effects are less than 10^{-2} $(\mu-1)$ for $L/D\geq10$]. Without the symmetry of the long cylindrical geometry, the perturbation inside is closer to order $(\mu-1)$, and therefore could be significant at 1 ppm.

Our use of Eq. (21) (measured at a field of 3 kG) for the frequency conversion in g-IV (which operates at a field of approximately 1 kG) assumes that $\omega_p(H_2O)$ is directly proportional to the magnetic field. A detailed consideration of a possible nonlinear field dependence of $\omega_p(H_2O)$ has shown that any nonlinearity has an effect of less than ±1 ppm from 3 to 1 kG.[29] Because there are no current grounds to suspect an appreciable effect at these fields, we will assume that there is no error in Eq. (20) due to nonlinearity.

III. APPARATUS AND PROCEDURE

The higher magnetic field and smaller orbit radius of g-IV required the construction of an entirely new apparatus. The major design goals were (i) a 1-kG magnetic field of sufficient circular symmetry over a 1-cm radius orbit to permit trapping electrons for up to 4×10^4 cycles of ω_D (10^4 μsec) in a well with a relative depth of 100 ppm or less; (ii) field stability and mapping accuracy sufficient to permit knowledge of the field to ±1 ppm over the course of a 24-h data run; and (iii) timing and control electronics accurate enough to introduce negligible error. Figure 3 shows an over-all diagram of the apparatus.

A. Solenoid and Magnetic Field Regulators

The magnetic field is generated by a precision solenoid, consisting of 12 layers of 0.110×0.200-in. rectangular copper wire wound on an aluminum form 24.0 in. in diameter by 89.0 in. in length. Two additional coils connected in series with the main winding produce the magnetic well field configuration. The axial position of these coils is adjustable to permit varying the well depth. At the

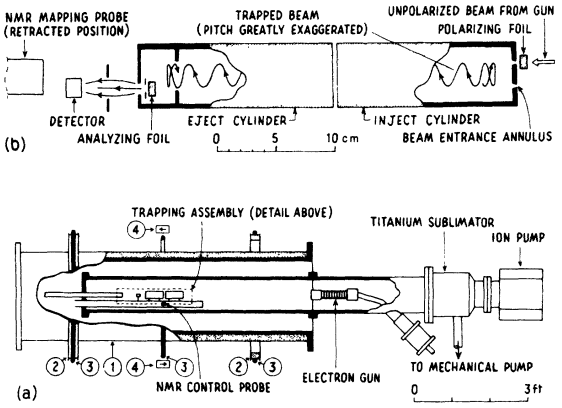

FIG. 3. Apparatus. (a) Over-all scale diagram: (1) solenoid winding, (2) well shaping coils, (3) field control windings, (4) gradient compensation coils. The gradient coils are mounted with opposing magnetic moments, as indicated by the arrows. (b) Components in the trapping region. The polarizing and analyzing foils are inclined at 45° to the plane of the diagram.

maximum field used in g-IV (1.2 kG), the solenoid draws 28 A at 800-V dc. The current through the windings is regulated to ±1 ppm short term (10 sec) and ±10 ppm long term (1 week) by a conventional shunt-stabilized current regulator.[21]

The solenoid is cooled by circulating an ethylene glycol solution between the inner and outer sleeves of the coil form. The entering coolant temperature is maintained at (10±0.2)°C by a reciprocating water chiller. Precise control of the coolant temperature is necessary in order to minimize field fluctuations due to thermal expansion of the solenoid.

The magnetic field in the trapping region is stabilized by an NMR servoregulator. The sensing probe is excited by a marginal oscillator that can be phase-locked to harmonics of a 0.5-MHz crystal-derived signal. The audio output of the marginal oscillator is detected by a lock-in amplifier, which in turn controls the current in a set of field stabilization windings (Fig. 3). The average fluctuation of the magnetic field in the trapping region is less than 1.0 ppm rms. The residual field fluctuation is due primarily to slight variations in the solenoid geometry with coolant temperature and flow. Figure 4 shows a typical chart-recorder trace of the magnetic field during a data run, monitored at a point 33 cm from the center of the trapping region.

A pair of small coils mounted with opposing magnetic moments on either side of the solenoid (Fig. 3) is used to provide an adjustable field gradient perpendicular to the z axis. This gradient is of the form $\partial B_z/\partial x$. The orientation of the gradient can be changed by rotating the coil pair around the solenoid axis, and the magnitude can be varied by changing the current through the coils. The coils produce a maximum field gradient of 5 ppm/cm.

B. Field-Mapping System

The magnetic field in the trapping region is mapped as a function of z using a second NMR probe. The trapping-cylinder assembly is rotated aside to permit the mapping probe to be extended into the trapping region. The probe is arranged with O-ring seals so that mapping may be accomplished without disturbing the vacuum, thus permitting field maps to be obtained immediately before and after an asymmetry data run.

The water sample of the mapping probe is a 0.2M solution of $CuSO_4$ in a toroidal glass container. The sample is 1.0 cm in length, with a mean radius of 1.0 cm, and 0.2 cm in thickness, corresponding to the range of radii occupied by the trapped electrons. The rf coil is wound around the sample in a toroidal configuration, and is excited by a conventional Pound-Knight marginal oscillator. The audio output of the oscillator is detected with a lock-in amplifier. The lock-in error signal is used to fine-tune the marginal oscillator frequency, thus permitting the oscillator to be "locked" to the magnetic field frequency. The equivalent NMR frequency can then be read directly from a frequency counter.

The width of the NMR line is 20 ppm full width at half-maximum (FWHM), due to the $CuSO_4$ doping of the sample. A superimposed 85-Hz sweep field is used to modulate the field at the sample. The sweep amplitude is ±5 ppm relative to the main solenoid field. The signal-to-noise ratio at the lock-in output is greater than 100:1. The center of the line can be determined to better than ±1 Hz, or ±0.2 ppm. The line center was found to be essentially independent of the rf amplitude, the audio sweep amplitude, the presence of stray 60- and 120-Hz pickup, and the total gain of the servoloop. Ability to measure the field was limited by thermal drift of the solenoid (Fig. 4).

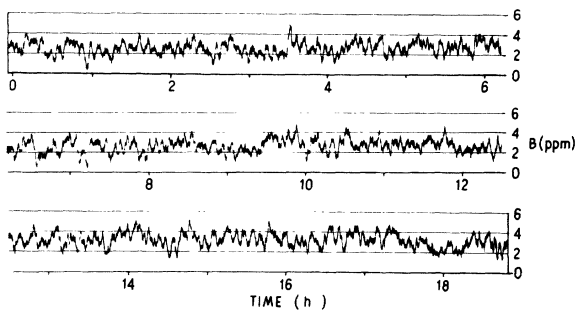

FIG. 4. Magnetic field stability. The field is monitored at a point 33 cm from the center of the trapping region.

The standard probe consists of a 1.2-cm-i.d. $\times$20-cm-long Plexiglas container filled with 0.2M $CuSO_4$. A 1-cm-long rf coil is wound at the center of the sample. The sample container is enclosed in a long concentric aluminum shield, with the rf connections brought out at the end of the shield. The sample, sample container, and shield therefore form a series of long concentric cylinders, ensuring that the resonance frequency will be independent (at a level of 1 ppm) of any uniform nonzero susceptibility of the materials used for the container and shield (Sec. II E). In order to test for possible nonuniform magnetic susceptibility (local magnetic contamination), three identical probes were fabricated from similar materials. No frequency shift between probes was detected at a level of ± 0.2 ppm. The electronics used with the standard probe are identical to the mapping electronics.

C. Vacuum System, Electron Gun, and Trapping Assembly

The pressure in the trapping region is maintained at 2×10^{-8} Torr or less by a 400 1/sec sputter ion pump and a 6000 1/sec titanium sublimator. A molecular-sieve trap on the roughing line prevents contamination of the vacuum system by backstreaming mechanical pump oil, and thus minimizes the possibility of the formation of insulating dielectric films (which could cause stray electric fields) on the interior of the trapping cylinders.

The electron gun is immersed in the main solenoid field, which provides focusing for the unpolarized electron beam. The gun is operated in a pulsed mode, and can produce up to 20 mA in a 1-mm-diam beam. The pulse length is nominally 200 nsec. The accelerating voltage (up to 120 kV) is provided by a conventional solid-state voltage doubler, operated from a Sorenson line-voltage regulator. High-voltage drift is less than $\pm 2\%$ after a 1-h warmup period. Ripple is less than $\frac{1}{2}\%$, with no corona or other transient fluctuations. The accelerating voltage is monitored by a resistive voltage divider. This network was checked against a second external divider. The two agree to 1.5%. The estimated uncertainty in the accelerating voltage is $\pm 3\%$.

The trapping cylinders and scattering foils are shown in Fig. 3. The cylinders are fabricated from copper, while the foil holders and baffles are brass and phosphor bronze. All interior surfaces are sprayed with an isopropanol suspension of colloidal graphite (Aerodag-G, available from Acheson Colloids Co., Port Huron, Michigan) in order to provide a uniform surface potential over the interior surface of the assembly. The partially polarized electrons enter the trapping region through an annulus of 1.0-cm mean radius and 0.2-cm width located in the end of the injection cylinder. This annulus, together with a baffle of 1.1-cm radius in the eject cylinder (Fig. 3), defines the location of the trapped beam. A series of apertures at the eject-cylinder end of the assembly allows electrons which scatter through $(90\pm15)^\circ$ at the analyzing foil to reach the detector. The scattering foils are commercial 23 k gold leaf, approximately 10^{-5} cm in thickness (220 μg/cm^2). The over-all efficiency of the first scattering is $(2\pm1)\times10^{-6}$, while the larger solid angle used in the second scattering increases the analyzing efficiency to $(1\pm0.5)\times10^{-4}$.

The materials used to fabricate the trapping assembly were checked for magnetic contamination with a pair of NMR probes placed in the solenoid field. If the object to be tested is brought near one of the probes, any magnetic properties will result in a frequency shift between the probes. Shifts as small as ±0.1 ppm can be detected. The complete trapping assembly affects the field by less than ±1.0 ppm over the useful portion of the trapping region (Sec. III F).

D. Timing and Detection Electronics

The timing of the various pulses necessary to inject, eject, and count the beam is established by a time-interval generator (TIG). This device may be programmed to produce a sequence of 3 pulses separated by multiples of 0.100 μsec, up to a maximum interval of 9999.9 μsec. The output of a precision 5-MHz crystal oscillator is doubled and shaped into a 10-MHz clock pulse signal. Selected pulses of the clock signal are gated to the desired outputs at times determined by preset digital counters. The output pulses are separated from the clock signal by a single emitter-coupled logic gate. The absolute accuracy of the time interval between the initial and delayed pulses is ±0.2 nsec $\pm$ 1 part in 10^7, as verified with a Hewlett-Packard 5360A-5379A computing counter. The rms jitter was less than 0.1 nsec, while long-term stability over a 5-day interval was better than ±0.2 nsec. For typical time intervals used in g-IV (2000–5000 μsec), the relative uncertainty from TIG is less than ±0.1 ppm.

The pulse system that controls the trapping (Fig. 5) operates at a repetition rate which may be varied from 100 to 1000 Hz. A single machine cycle consists of the following events. (i) TIG produces an electron gun trigger pulse at $T=-0.3$ μsec, resulting in a 200-nsec burst of scattered electrons drifting into the trapping region at $T=0$. (ii) TIG produces an inject trigger at $T=0$. The inject pulser applies a +20-V 100-nsec pulse to the inject cylinder. Electrons which drift across the cylinder gap during this 100-nsec interval are trapped. (iii) At the desired ejection time T_e, TIG produces an eject trigger, which initiates the following sequence of

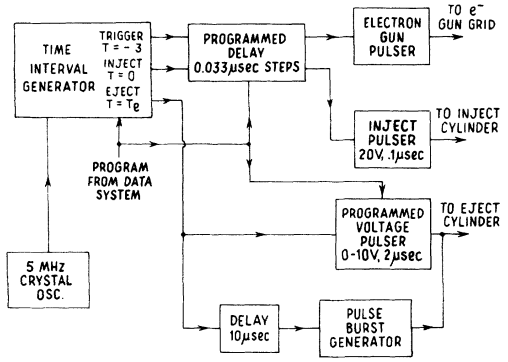

FIG. 5. Timing system.

events: (a) The eject pulser applies a 2.0-μsec pulse of voltage $+V_e$ to the eject cylinder, ejecting that half of the trapped beam in the inject cylinder at T_e; (b) the counting electronics are gated on at $T = T_e$; (c) at $T = T_e + 10$ μsec, a 50-μsec burst of +10-V pulses at a 1.5-MHz repetition rate is applied to the eject cylinder, thus clearing the trap of electrons prior to the next machine cycle.

The counting system consists of a 700-μ-thick silicon surface-barrier detector followed by a charge-sensitive preamplifier. A timing discriminator with threshold discrimination produces a fast-timing pulse (STOP) derived from the leading edge of the preamplifier output. Energy discrimination using a single-channel analyzer ensures that only elastically scattered electrons are counted. A coincidence between STOP and the SCA output produces a delayed logic pulse (STORE) which is used to initiate the storage of data in the data system. The fast-timing signal is also routed to the data system.

Noise in the detector and preamplifier results in a 10-nsec FWHM time-jitter spectrum in STOP. Time slewing due to pulse-height variation is less than 5 nsec over the SCA window. The variation of the average electron pulse height between inner and outer trapping times is less than ±20% of the SCA window. The effect of time slewing is therefore less than ±1 nsec.

E. Data System

The data system (Fig. 6) is used to (i) measure the asymmetry function $[R^K(T)]$ as a function of T, (ii) measure the ejection function $[N(V)]$ as a function of V, (iii) accumulate asymmetry and ejection data at two preset trapping times in a sequential manner, and (iv) store the asymmetry and ejection data. During the course of a data run, a program generator (Fig. 6) controls the various pulse generators and interface electronics that establish the trapping time, ejection voltage, and data storage location. The data are accumulated in the form of counts stored in specific channels of a multichannel analyzer (MCA) memory.

Measurement of the Asymmetry Function

The time of arrival of an electron is digitized by counting the number of cycles of a 30-MHz clock signal that occur between the eject trigger and STOP. The clock signal is synchronized with the eject trigger, so the number of clock pulses identifies the time interval in which the electron arrives. The pulses are counted by a scaler, whose binary output is used as the first four bits of the MCA address.

The program generator contains two index registers i and m, where $i = 1$ or 2 and $m = 1, 2, \ldots, 8$. The contents of these registers determine the trapping time. The ejection time is switched between two preset times T_1 and T_2, according to the state of index i. The injection time is varied by delaying the gun trigger and injection pulses $(8-m) \times (0.0333)$ μsec with respect to $T = 0$. The total trapping time is therefore $T_{m,i} = \{T_i - (8-m)(0.0333)\}$ μsec. The indices i and m also determine the remaining four bits of the MCA address, thus dividing the MCA memory into 16 groups, each corresponding to a specific $T_{m,i}$. Within each group, the 16 individual channels represent successive intervals of 33.3 nsec starting at $T = T_1$ or $T = T_2$, and thus correspond to the K intervals of Eq. (23). The logic signal STORE is used to store one count in the channel addressed by the electron's time of arrival. The distribution of counts in the channels of each group is therefore $R^K(T_{m,i})$, as defined by Eq. (23) for $T_e = T_{m,i}$.

Measurement of the Ejection Function

During the accumulation of ejection-function data, the ejection voltage V_e is varied under the control of the program index m in eight equal steps V_m from $\frac{1}{8}V^*$ to V^*. The counts ejected by the mth ejection voltage are stored in channels of the memory. The accumulated data consists of eight values of $N(V_m)$ for $T = T_1$ and eight values for $T = T_2$.

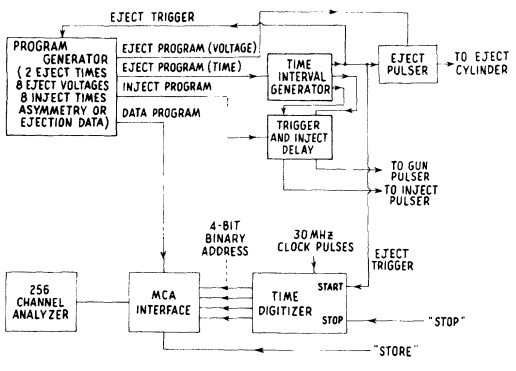

FIG. 6. Data system.

Data are accumulated in the following sequence.

(i) i and m are set to 1. Asymmetry data are accumulated in channels 0–15 (except 1, which is inhibited) for 100 machine cycles.

(ii) m is set to 2. Asymmetry data are accumulated in channels 16–31 (except 17) for 100 machine cycles.

(iii) This sequence continues for $m = 3, 4, \ldots, 8$, with data stored in the corresponding group of channels.

(iv) m is reset to 1 and i is set equal to 2. Steps (i)–(iii) are repeated, except that data are stored in channels 128–143, 144–159, etc.

(v) Steps (i)–(iv) are repeated nine times. The tenth time, the data system switches to acquiring ejection-function data. The program index m now controls the ejection voltage V_m, and all counts are stored in the first channel of each group (i.e., in channel 1 for $m = 1$, channel 17 for $m = 2$, etc.). Steps (i)–(iv) are repeated once for ejection data.

(vi) The data system is returned to step (i) to repeat the complete sequence.

Sequential Accumulation of Data

Sequential accumulation of data serves to average the effects of fluctuations in the intensity of the trapped beam as a function of time. Small fluctuations in the perpendicular field gradient result in corresponding variations in the beam intensity. Although the mean intensity (averaged over a 10-min interval) is reasonably constant, the instantaneous intensity can vary from the mean by up to ±50% over a period of 30 sec. The cyclical accumulation averages out the effects of this variation. At a typical machine rate of 200 Hz, the data system program changes every $\frac{1}{2}$ sec (i.e., $m \rightarrow m + 1$), so that a complete cycle through the sequence of trapping times takes place rapidly compared with variations in the beam intensity. Sequential accumulation of data has the additional advantage that slow drifts of the experimental parameters affect both inner and outer trapping times equally. Since data are taken at both trapping times (in essence) simultaneously, the electric and magnetic field experienced by the electrons are identical for each trapping time, and any timing drift in the preamplifier, timing discriminator, or time digitizer cancels out, since only time differences are significant.

The data system was checked for electronic asymmetries by recording an asymmetry curve with all programs preset to the same trapping time. The counting rate would then be expected to be independent of the program number. No statistically significant asymmetry was found at a level of ±0.1%.

F. Experimental Procedure

The basic experimental procedures in g-IV are (i) trapping of a polarized electron beam, (ii) point-by-point measurement of the magnetic field over the region occupied by the trapped beam (field mapping), (iii) measurement of the asymmetry and ejection functions, and (iv) calibration of the mapper probe against the standard NMR probe. A combination of the first three procedures constitutes a data run for measuring the quantity a'. A single probe calibration is sufficient for the entire series of runs.

Electron Trapping

Figure 2 shows a typical magnetic field used for one of the 5-MHz data runs. At the other nominal magnetic field values, the relative depth (60 ppm) and shape of the well were maintained to 5%. The field was, of course, remapped for each data run.

The radial symmetry of the magnetic field controls the drift of the trapped electrons perpendicular to the z axis. In order to obtain a stable trapped beam, it was necessary to introduce an external perpendicular field gradient of approximately 5 ppm/cm to cancel the asymmetry of the main solenoid field. The exact orientation and magnitude of the gradient that were required varied somewhat from day to day, depending on the magnitude and previous history (cycling) of the solenoid power level, as well as on coolant temperature and flow. The intensity of the trapped beam fluctuated in a more or less random manner as a function of time. Apparently, small variations in coolant temperature, flow, and turbulence result in minute changes in the solenoid temperature, with corresponding geometrical variations from thermal expansion. This causes variation of the perpendicular gradient, with corresponding variation in beam intensity.

After proper adjustment of the external gradient, the trapped beam intensity was found to be essentially independent of trapping time, except from the effects of the Ω motion (Sec. II A) and scattering from the residual gas molecules in the trapping region. The maximum trapping time used in the data runs was 5900 μsec; less than 10% of the beam was lost owing to scattering at this trapping time.

Field Mapping

The toroidal sample of the mapping probe occupies the same range of radii as the trapped electrons. Since the natural linewidth of the $CuSO_4$ solution (20 ppm FWHM) is considerably greater than the maximum field variation over the sample volume (< 5 ppm), the center of the resonance line represents, to a high accuracy, the spatial average of the magnetic field over the sample volume. The resonance frequency of the probe is assigned to be the value of the magnetic field at the axial midplane of the sample. A field map consists of a

series of measurements of the probe resonance frequency, with the probe positioned at 1.0-cm intervals along the z axis. The series of 32 measurements for a complete field map requires about 5 min to complete.

Magnetic Properties of Trapping Assembly

During the data runs, the magnetic field is mapped with the trapping assembly rotated to one side in the mapping position. When the assembly is returned to the data run position, the residual magnetic properties of the cylinder assembly can be expected to affect the magnetic field inside. A modified version of the field-mapping procedure was used to measure the field difference between the two positions.[21] The measured values of this shift are then used to correct the field maps obtained during the data runs. After making this correction, the residual uncertainty in the time- and ensemble-averaged magnetic field due to the effects of the cylinder assembly is ±0.2 ppm.

Asymmetry and Ejection Data

The accumulation of asymmetry and ejection data is automatically accomplished by the data system, as described in Sec. III E.

Mapper Probe Calibration

The mapper probe was calibrated against each of the three standard probes. The field at the center of the solenoid is homogeneous to ±0.2 ppm over the sensitive volumes of the probes. After careful positioning of the probes in the region of maximum homogeneity, the ratio $\omega_p(S)/\omega_p(M)$ was measured by repeated interchange and comparison of the two probes.

Data Run Procedure

Data runs were divided into two groups, designated by numbers less than 100, and greater than 100. The first group of runs was completed before the data control and recording system was completely automated, so these runs differed somewhat in the actual sequence of events used. The 100 series runs comprised the majority of the data used to measure a. After the beam intensity had been peaked and the field mapped, the data system was used to accumulate asymmetry and ejection data. During the course of the run, the beam intensity was monitored. If the average intensity decreased by more than 30%, a slight readjustment of the gradient was made to repeak the beam. This adjustment was required in about one-fourth of the runs. The maximum uncertainty in the time- and ensemble-averaged field introduced by this procedure was ±0.2 ppm. The magnetic field was also monitored during the run (Fig. 4). After sufficient data had been accumulated (about 10^6 total counts), the field was remapped. A typical run required about 24 h.

The preliminary runs involved a similar procedure, except that data were taken at each trapping time without the automatic switching feature of the data system.

Table I contains a summary of several experimental parameters at each nominal magnetic field.

IV. DATA ANALYSIS

In order to calculate a' from the experimental data, it will be convenient to rewrite Eq. (12) in the form

$$a' = \frac{1.520\,994\,5\times10^{-3}\,N\,(1+\epsilon)}{\{N\langle[\tau_D]\rangle\}\langle[f]\rangle}\left(1+\frac{\langle[\beta_z^2]\rangle}{2}\right), \quad (22)$$

where $\langle[\tau_D]\rangle = 2\pi/\langle[\omega_D]\rangle$, $\{N\langle[\tau_D]\rangle\}$ is the time between the inner and outer maxima of the asymmetry curve (in μsec), N is the number of cycles, $\langle[f]\rangle = \langle[\omega_p(M)]\rangle/2\pi$ (in MHz), and $1+\epsilon = \omega_p(M)/\omega_p(S)$. In the material that follows, all errors are ±1 standard deviation (68% confidence level) unless otherwise noted.

A. Evaluation of Difference Period

Asymmetry Curve Fitting and Statistical Timing Error

A nonlinear estimation program (IBM S3226-SY) is used to fit the data of $R^K(T_{m,i})$ vs $T_{m,i}$ to the cosine function of Eq. (18). The program returns best-fit values for R_0^K, δ_K, and ϕ_K, together with the estimated standard deviations $\sigma(R_0^K)$, $\sigma(\delta_K)$, and $\sigma(\phi_K)$ (these errors arise from the statistical fluc-

TABLE I. Experimental parameters for the data runs.

NMR frequency	(MHz)	5.0	4.5	4.0	3.5
Magnetic field	(kG)	1.17	1.06	0.94	0.82
Electron energy	(keV)	108	89	73	56
Ejection voltage	(V)	4.0	3.2	2.8	2.4
$\Delta B/\Delta V$ (Sec. II C)	(Hz/V)	49.9	54.6	59.1	65.6
Difference frequency period	(nsec)	262	292	328	376
Axial oscillation period	(nsec)	650	700	740	820
X (Sec. II B)	(kG^{-1})	1.02	1.31	1.69	2.28

tuation in R^K). The standard deviations are estimated by numerical evaluation of the matrix of the residuals (the error matrix; see the Appendix). Proper convergence of the least-squares fit to a true minimum was checked by using the program to fit data where an exact solution to the least-squares problem could be calculated by analytic methods (e.g., if the data points are spaced at intervals of $\frac{1}{2}\pi$).[20] The values of $\sigma(R_0^K)$, $\sigma(\delta_K)$, and $\sigma(\phi_K)$ estimated by the program were found to be in excellent agreement with the *a priori* estimates

$$\sigma^*(R_0^K) = (R_T^K)^{1/2} , \tag{23a}$$

$$\sigma^*(\delta_K) = \sqrt{2}\ R_0^K\ (R_T^K)^{-1/2} , \tag{23b}$$

$$\sigma^*(\phi_K) = \sqrt{2}\,\delta_K\,(R_T^K)^{-1/2} , \tag{23c}$$

as derived using the method of maximum likelihood (Appendix). In Eq. (23) we have

$$R_T^K = \sum_{m=1}^{8} R^K(T_{m,i}) ,$$

i.e., the total number of counts in the Kth curve.

Equations (19a)–(19c) are then used to calculate R_0, δ, and ϕ. The standard deviations $\sigma(R_0)$, $\sigma(\delta)$, and $\sigma(\phi)$ are calculated from $\sigma(R_0^K)$, $\sigma(\delta_K)$, and $\sigma(\phi_K)$ by applying the theory of propagation of errors to Eqs. (19a)–(19c), e.g.,

$$\sigma^2(\phi) = \sum_k \left\{ \left(\frac{\partial\phi}{\partial R_0^K}\right)^2 \sigma^2(R_0^K) + \left(\frac{\partial\phi}{\partial\delta_K}\right)^2 \sigma^2(\delta_K) + \left(\frac{\partial\phi}{\partial\phi_K}\right)^2 \sigma^2(\phi_K) \right\} . \tag{24}$$

Again, the standard deviations calculated in this manner are in excellent agreement with *a priori* estimates of $\sigma(R_0)$, $\sigma(\delta)$, and $\sigma(\phi)$, as obtained from Eqs. (23a)–(23c), using $R_T = \sum_K R_T^K$ as the total number of counts in the run.

A typical data run and the fitted curves are shown in Fig. 7. The principal parameters of interest are ϕ and $\sigma(\phi)$, which determine the position of a maximum to be at time $T_i \pm \sigma(T_i)$. For a single data run, the phase error at each trapping time is approximately ± 0.1 rad, corresponding to a ± 5-nsec uncertainty in the position of the maximum. The relative statistical error in $\{N\langle[\tau_D]\rangle\}$ for a single run was typically ± 2 to ± 4 ppm.

Absolute and Total Timing Error

The total absolute timing error is the rms sum of (i) the absolute error from the time-interval generator, ± 0.1 ppm, (ii) the error from time slewing (Sec. III D), ± 0.5 ppm, and (iii) slow timing drift in the discriminator and time digitizer, ± 1.0 ppm. Error (iii) is present only for runs 001–015. In runs 114–155, the automatic switching between inner and outer trapping times eliminated the effect of slow timing drift.

The total error in $\{N\langle[\tau_D]\rangle\}$ is the rms sum of the statistical timing error and errors (i)–(iii) above. Statistical error contributes approximately 80% of the total timing error in a single data run.

Cycle Counting

The following procedure was used to determine N without an explicit counting of all of the cycles between the selected maxima of R. Two asymmetry curves separated by 200 μsec were used to establish the time interval $\{N_1\langle[\tau_D]\rangle\}$ to an accuracy of ± 50 ppm. Evaluation of field-map and ejection-function data (Sec. IV B) established $\langle[f]\rangle$ to an accuracy of ± 1 ppm. The product $\{N_1\langle[\tau_D]\rangle\langle[f]\rangle\}$ was therefore known to ± 50 ppm. The results of g-III were used to identify N_1. The *absolute limits* of a' expected in g-IV were taken to be $(1\,159\,500 \pm 500)\times 10^{-9}$, where the greatly increased error (15 times the reported accuracy of g-III) allows for a 400-ppm shift in a' owing to the possible presence of a large (~ 100 mV/cm) time-average radial electric field in g-IV. Substituting this result and $N = 1$ in Eq. (22), the result of g-III becomes $\{\langle[\tau_D]\rangle\langle[f]\rangle\}_{WC} = 1.3117 \pm 0.0005$, so that

$$N_1 = \frac{\{N_1\langle[\tau_D]\rangle\langle[f]\rangle\}}{\{\langle[\tau_D]\rangle\langle[f]\rangle\}_{WC}} = 761.95 \pm 0.35 .$$

Since the uncertainty is an absolute limit of error, N_1 was identified to be 762. A new value for $\{\langle[\tau_D]\rangle\langle[f]\rangle\}$ was then calculated from the g-IV data, using $\{\langle[\tau_D]\rangle\langle[f]\rangle\}_1 = \{N_1\langle[\tau_D]\rangle\langle[f]\rangle\}/762$. The standard deviation of this quantity was ± 50 ppm.

The cycle counting procedure was then repeated using a new pair of asymmetry curves separated by 600 μsec, yielding a value of $\{N_2\langle[\tau_D]\rangle\langle[f]\rangle\}$ accurate to ± 20 ppm. Proceeding in a similar manner, we have

$$N_2 = \frac{\{N_2\langle[\tau_D]\rangle\langle[f]\rangle\}}{\{\langle[\tau_D]\rangle\langle[f]\rangle\}_1} = 2287.05 \pm 0.3\ (\pm 3\sigma) ,$$

and therefore $N_2 = 2287$. A third repetition of this

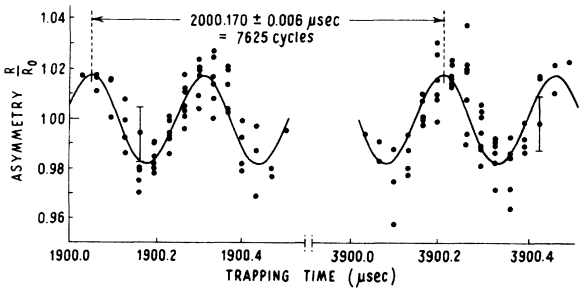

FIG. 7. Typical asymmetry data and fitted curves.

procedure using the asymmetry curves of the first data run (separated by 2000 μsec) was used to obtain $N = 7623.8 \pm 0.4$ ($\pm 3\sigma$). Therefore, N was identified to be 7624. Since the standard deviation of N is approximately 0.15 cycle, the probability of a one-cycle miscount is less than 10^{-6}, assuming that N is distributed normally.

The cycle counting procedure was performed for runs 001–008 (5 MHz) and repeated for runs 009–012 (3.5 MHz). The results indicated that the value $\{\langle[\tau_D]\rangle\langle[f]\rangle\} = 1.3116 \pm 0.00001$ was sufficiently accurate to identify N within ± 0.1 cycle in all succeeding runs.

A plot of $a'(X)$ vs X provides an independent check for the possibility of a one-cycle miscount (Fig. 8). Each point represents the result of a single data run. If the true number of cycles for the ith run were $N_i' = N_i \pm 1$ instead of the most probable value N_i, the values of a_i' would be revised as shown. If $N_i' = N_i \pm 1$, (i) the dispersion of a_i' at each nominal field is greatly increased (note the complete splitting of the data into two distinct groups at 5.0 and 4.0 MHz), and (ii) there is no linear fit to the data that would give a statistically acceptable dispersion. The data are statistically acceptable only if $N_i' = N_i$. The possiblity of a one-cycle miscount is therefore completely negligible.

B. Evaluation of the Time- and Ensemble-Averaged Quantities

Calculation of Density Function

The density function is calculated from the ejection data of $N(V_m)$ vs V_m by a graphical method. The quantity $N(V_m)/N(V^*)$ is plotted as a function

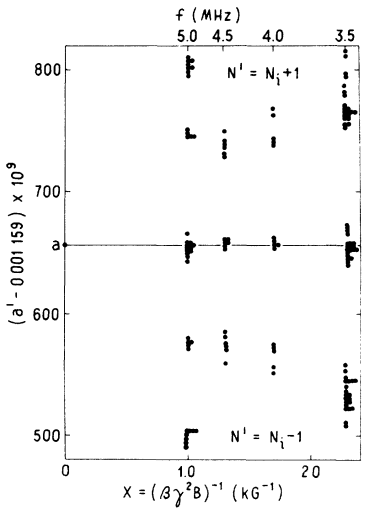

FIG. 8. Effect of a one-cycle miscount. Each point represents the results of an individual data run. The error in each point is approximately twice the diameter of the point (see Sec. IV A for a complete explanation).

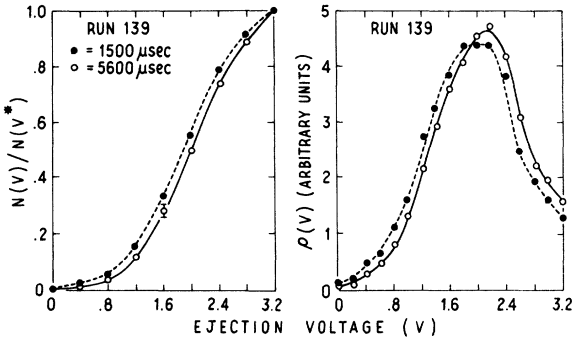

FIG. 9. Typical ejection data and density functions.

of V_m/V^*. The slope of a smooth curve drawn by eye through the data points is then evaluated at 17 equal voltage intervals to yield a series of values of $\rho(V)$. A typical set of ejection data and the derived density functions are shown in Fig. 9.

Calculation of Time and Ensemble Averages

The time and ensemble averages are evaluated numerically. After the raw field-map data of $B(z)$ vs z at 1-cm intervals are corrected for the residual magnetic effect of the trapping cylinder assembly, additional values of B are interpolated at 0.05-cm intervals. The resulting array of data points is used to evaluate Eqs. (7), (14), and (15) by Simpson's method. The contribution of the end segments (turning points of the motion) is calculated by an explicit integration formula, which assumes that B is a linear function of z in the last 0.05 cm of the motion. Without the explicit integration of the end segments, a substantial error {up to 20% of τ, $B(z_1) - [B]$, or $[\beta_z^2]$} can arise from purely numerical integration, owing to the rapid increase of the $B(z_1) - B(z)^{1/2}$ integrand near the end points. For example, refined numerical calculations of $[B]$ and $[v_z^2]$ for g-III were responsible for about one-half the change in a reported in Ref. 16. The quantities $[B(B')]$, $[\beta_z^2(B')]$, and τ are evaluated at a series of levels in the well. After $\rho(V)$ is converted to $\rho(B')$ and normalized over the interval $B_{\min}$–$B_{\max}$, further numerical integrations are used to evaluate Eqs. (16) and (17).

Error in the Time- and Ensemble-Averaged Field

Explicit uncertainties contributing to error in $\langle[f]\rangle$ are (i) random and absolute error in the NMR field measurements, (ii) uncertainty in the density function, (iii) uncertainty in the voltage to well-depth conversion, and (iv) numerical error in evaluating the time and ensemble averages.

The absolute error in determining the NMR frequencies was ± 1 Hz, ± 0.1 ppm. In addition, a

random error of ±1.0 ppm was present owing to noise and slow drift of the field during the field maps and data runs (Fig. 4). The effect of this variation on the time-average field is approximately ±0.3 ppm, as estimated from the standard deviation of a series of repeated field maps.

The ejection function was observed to vary slightly from run to run, and as a function of trapping time. In addition to a random variation from run to run (approximately 50% of which was due to counting statistics), there was a systematic relative loss of electrons from the upper levels of the well with increasing trapping time (Fig. 9). This phenomenon is probably due to scattering from the residual gases in the trapping region. Electrons near the top of the well will be lost more rapidly by scattering than those near the bottom, since the necessary scattering angle for an electron to leave the trap decreases to zero at the maximum level of the trap.

The plausibility of determining $\langle [f] \rangle$ to approximately 1 ppm in the g-IV trap can be illustrated as follows. The maximum and minimum levels in the well have time-average fields differing by 22 ppm (Fig. 2). The absolute limits of uncertainty in $[f]$ are therefore ±11 ppm. This assumes, however, that all electrons could be either at the very top or bottom of the well. If, as is much more likely, the electrons are distributed in some reasonably smooth but *unspecified* way, we can divide the limits of error by about a factor of 2, and thus obtain $\sigma(\langle [f] \rangle) \cong 6$ ppm. The uncertainty in $\langle [f] \rangle$ can be further reduced to less than ±1 ppm if ρ can be directly measured to an accuracy of order 10%.

The experimental uncertainty in $\langle [f] \rangle$ was determined by statistical analysis of field and ejection data from runs 001–015. For these runs, ejection data were taken immediately before and after each asymmetry data segment. The field was mapped three times during each run. The time- and ensemble-average field was calculated for various combinations of the field and density data. The standard deviation of $\langle [f] \rangle$ was approximately 1.0 ppm. We estimate that this uncertainty is the rms sum of (i) random drift in the field, ±0.3 ppm, (ii) random variation in ρ, ±0.7 ppm, and (iii) systematic variation of ρ with trapping time, ±0.6 ppm.

In runs 114–155, the value of $\langle [f] \rangle$ assigned to each run was the average of the four values obtained by combining the density function at each trapping time with the two field maps from each run. The uncertainty was assigned to be ±1.0 ppm.

Uncertainty in the energy of the trapped electrons results in a corresponding uncertainty in the voltage to well-depth conversion. The uncertainty in the accelerating voltage is ±3%. Additional uncertainty, estimated to be about 1 keV, arises from energy loss upon passing through the polarizing foil.[21] This estimate is confirmed by the fact that the counting rate as a function of accelerating voltage exhibits a maximum within ±2 kV of the value expected for the 1.0-cm beam radius. The total uncertainty in the trapped electron energy is therefore taken to be ±5%, resulting in a ±5% uncertainty in $B_{\min}$, i.e., $\sigma(B_{\min}) = 0.05\ (B_{\max} - B_{\min})$. Error in V^* also contributes an additional uncertainty of ±3% in $B_{\min}$. The total rms uncertainty in $B_{\min}$ is therefore 6%. The corresponding uncertainty in $\langle [f] \rangle$ is ±0.7 ppm.

The numerical error in evaluating $\langle [f] \rangle$ is less than ±0.1 ppm. Several tests were made to ensure proper functioning of the computer program used to evaluate $\langle [f] \rangle$. These included calculating the time-average field for the function $B = k_1 (z/L)^2$, where the result $[B] = \frac{1}{2} k_1$ is exact. The numerical result agreed to 0.1% of the well depth (i.e., 0.1-ppm absolute error). The density integral portion of the program was checked using density functions that could be integrated analytically [e.g., $\rho(B') = \text{const}$, $\rho(B') = k_2 B'$]. Again, the absolute error was less than 0.1 ppm. The 1% agreement of the calculated and measured axial oscillation frequencies (Sec. II A) also constitutes a sensitive check for proper evaluation of the time-average integrals.

The total uncertainty in $\langle [f] \rangle$ is the rms sum of the various errors considered above. Some of these errors are absolute, that is, they will not be reduced by averaging. These are (i) absolute error in determining the NMR frequencies, ±0.3 ppm, (ii) uncertainty in $B_{\min}$, ±0.7 ppm, and (iii) uncertainty owing to the variation of ρ with trapping time, ±0.6 ppm. In addition, there are random errors from (i) random variation of ρ, ±0.7 ppm, and (ii) random variation of the magnetic field, ±0.3 ppm. The total random error is ±0.8 ppm; the total absolute error is ±1.0 ppm. Since the absolute error is common to all data runs, it will be included after averaging the results of the individual runs at each value of X.

Error in $\langle [\beta_z^2] \rangle$

The various uncertainties from field mapping and variations of ρ noted above are the principal sources of error in $\langle [\beta_z^2] \rangle$. An analysis similar to that made for $\langle [f] \rangle$ shows that the maximum error in $\frac{1}{2} \langle [\beta_z^2] \rangle$ is $\pm 0.1 \times 10^{-7}$, or 0.1 ppm of a.[21] The values of $\frac{1}{2} \langle [\beta_z^2] \rangle$ ranged from 1.0×10^{-6} to 2.5×10^{-6}. The uncertainty introduced by the axial velocity correction is therefore negligible.

Mapper Probe Calibration

The mapper probe was calibrated against the standard probe on two occasions, at the conclusion of runs 015 and 155. The sample container was replaced after run 015. There was no evidence for a frequency shift between the three standard probes at a level of ±0.2 ppm. The calibration factors

are $\epsilon = (1.3 \pm 0.2) \times 10^{-6}$ (runs 001–015) and $\epsilon = (1.1 \pm 0.2) \times 10^{-6}$ (runs 114–155). Since this correction is common to all data runs, the uncertainty will be included after extrapolating to obtain a.

C. Results of Individual Data Runs

The result a_i' of each data run is calculated using Eq. (22). The estimated error $\sigma^*(a_i')$ is the rms sum of the random uncertainties in $\{N\langle[\tau_D]\rangle\}$, ±2 to ±4 ppm; $\langle[f]\rangle$, ±0.8 ppm; and $\frac{1}{2}\langle[\beta_z^2]\rangle$, ±0.1 ppm. In the remainder of Sec. IV, the asterisk indicates that the standard deviation is an estimate based on *a priori* considerations. In Sec. IV D, we determine whether $\sigma^*(a_i')$ represents a satisfactory assessment of the total error in a_i'. Several parameters and the results of the data runs are given in Table II.

D. Systematic Error in a

In order to determine a from a_i', it is necessary to consider the dependence of a' on the electric fields assumed to be present in the trapping region. In particular, we make the hypotheses that $\langle[E_\perp]\rangle$ is (i) independent of X and (ii) constant during the entire series of runs. If these hypotheses are not completely valid, a certain amount of systematic error will arise in the extrapolation of a' vs X to determine a. In the following paragraphs, we will consider in detail the validity of hypotheses (i) and (ii). We will also consider several possible sources of systematic error and estimate the magnitude of the effect of each.

Since Eq. (12) is central to our final determination of a, a series of measurements were made to verify the dependence of a' on X and $\langle[E_\perp]\rangle$. This was accomplished by measuring a' as a function of an externally applied dc voltage on the injection cylinder (in addition to the usual injection pulse). The potential and electric field in the trapping region can be calculated from a power-series solution to the boundary value problem. The axial electric field perturbs the axial motion, while the radial electric field shifts the difference frequency.[21] In order to calculate the expected shift in a', both effects must be considered. Satisfactory agreement was found between theory and experiment (Fig. 10). This not only confirms the dependence of a' on X and $\langle[E_\perp]\rangle$, but also indirectly checks the orbit theory used to obtain $v_z(z)$, as well as the entire calculation of the time and ensemble averages. In particular, $\langle[E_\perp]\rangle$ is quite sensitive to small variations in $B_{\min}$ or ρ. A 3% decrease in $B_{\min}$ increases $\langle[E_\perp]\rangle$ by about 10%, while $\langle[B]\rangle$ decreases by only 1.5% of the relative well depth. Confirmation of the predicted dependence of a' on X therefore serves as a sensitive test for proper evaluation of the time and ensemble averages, which is, of course, essential to the projected final accuracy of g-IV.

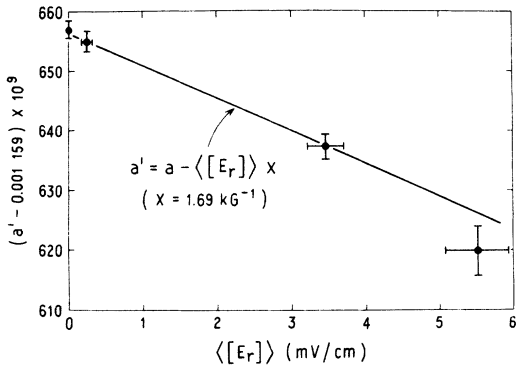

FIG. 10. Shift in a' as a function of an externally applied radial electric field. The solid line shows the predicted dependence.

Systematic Dependence of a' on X

Any systematic dependence of $\langle[E_\perp]\rangle$ on X or experimental parameters that vary with X will introduce systematic error in the extrapolated value for a. The results of the extrapolation (to be made later) show that $\langle[E_\perp]\rangle \sim 1$ mV/cm. Three possible sources of fields of this magnitude are (i) contact potentials between dissimilar materials exposed in the interior surface of the trapping assembly, (ii) space charge of the trapped electrons, and (iii) space charge of ions created from ionization of residual gases in the trapping region. All three have been considered in detail elsewhere.[21] We conclude that (a) only contact potentials could be responsible for electric fields corresponding to the observed values of $a_i' - a$, and (b) the only appreciable systematic dependence of $\langle[E_\perp]\rangle$ on X is from the effect of the space charge of the trapped electrons.

Systematic Effect of Space Charge

The number of trapped electrons is estimated to be approximately 5×10^3, as calculated from the average counting rate of 0.5 electrons per machine cycle, an analyzing efficiency of 10^{-4}, and an ejection efficiency of $\frac{1}{2}$. A computer calculation that takes into account the actual radial and axial charge distribution shows that $\langle[E_\perp]\rangle = -0.1$ mV/cm is a conservative upper limit to the electric field from space charge.[21] In order to maintain an approximately constant number of trapped electrons, the unpolarized beam current was decreased by a factor of 3 from 5.0 to 3.5 MHz to offset the threefold increase of the Mott cross section from 108 to 56 keV. The residual systematic variation in the number of injected electrons was less than 50%. The absolute number of trapped electrons varied by less than a factor of 2 owing to random varia-

TABLE II. Results of the data runs.

Run	N	$N\langle[\tau_D]\rangle$ (μsec)	$\sigma^*(N\langle[\tau_D]\rangle)$ (ppm)	$\langle[f]\rangle$ (MHz)	VC[a]	A'[b]	$\sigma^*(a')$ (ppm)
001	7624	1999.8843	3.2	5.000 094 0	2.70	656.1	3.4
002	7624	1999.8811	3.5	5.000 094 9	2.70	657.8	3.7
003	7624	1999.8940	3.4	5.000 093 9	2.70	650.5	3.5
004	7624	1999.9024	3.3	5.000 092 6	2.80	646.1	3.4
005	7624	1999.9081	3.2	5.000 093 5	2.75	642.5	3.4
006	7624	1999.8841	4.0	5.000 098 0	2.40	656.5	4.0
007	7624	1999.8852	3.6	5.000 104 8	2.40	652.8	3.9
008	7624	1999.8797	3.6	5.000 101 7	2.40	656.6	3.9
114	13 724	3599.9620	4.3	5.000 106 5	2.15	665.1	4.5
116	13 343	3500.0480	1.9	5.000 103 7	2.40	657.2	2.2
117	12 581	3300.1737	1.6	5.000 107 3	2.50	653.5	1.8
118	12 581	3300.1708	2.1	5.000 099 6	2.45	656.2	2.3
120	12 961	3399.8489	1.8	5.000 107 5	2.40	654.7	2.0
015	12 008	3499.8326	2.1	4.500 125 6	2.60	653.1	2.3
136	15 783	4600.1276	2.4	4.500 075 3	2.10	655.3	2.6
137	16 126	4700.0904	1.9	4.500 069 2	2.05	658.9	2.1
138	14 411	4200.2408	1.5	4.500 061 2	1.85	659.3	1.8
139	14 068	4100.2746	1.9	4.500 061 9	1.90	657.8	2.1
140	14 067	4099.9893	1.3	4.500 063 4	1.90	655.6	1.6
013	10 980	3600.2345	2.9	4.000 084 9	2.00	662.0	3.1
014	10 980	3600.2417	2.5	4.000 094 0	2.10	657.1	2.8
133	11 284	3699.9526	2.2	4.000 059 1	1.60	656.4	2.4
134	11 589	3799.9666	1.7	4.000 063 1	1.50	653.1	2.0
146	11 894	3899.9744	2.2	4.000 052 0	1.65	656.5	2.5
147	11 894	3899.9791	1.6	4.000 051 3	1.60	655.2	1.9
148	11 894	3899.9656	1.5	4.000 050 8	1.60	659.4	1.8
009	8006	3000.0757	11.0	3.500 071 9	1.80	672.6	11.1
010	8006	3000.1080	7.3	3.500 049 8	1.45	667.0	7.4
011	8006	3000.1455	9.9	3.500 049 0	1.45	652.8	9.8
012	8006	3000.1419	8.0	3.500 048 0	1.50	654.6	8.1
123	10 674	3999.9791	8.9	3.500 047 6	1.30	642.7	9.0
124	10 407	3899.8300	12.9	3.500 043 1	1.30	670.5	13.0
125	10 140	3799.8807	3.5	3.500 043 2	1.30	640.2	3.7
126	10 674	3999.9833	2.5	3.500 046 3	1.20	641.8	2.7
127	10 140	3799.8605	3.8	3.500 046 1	1.20	645.3	4.0
130	10 407	3899.8807	2.7	3.500 043 1	1.25	656.8	2.9
131	10 407	3899.8700	4.6	3.500 047 2	1.25	658.7	4.8
132	9873	3699.7888	2.8	3.500 047 2	1.25	650.0	3.0
141	10 407	3899.9141	3.5	3.500 038 1	1.35	648.7	3.7
142	10 674	3999.9475	3.7	3.500 039 0	1.40	654.8	3.9
143	10 674	3999.9427	5.2	3.500 039 6	1.45	656.1	5.3
144	10 407	3899.9243	4.0	3.500 041 7	1.40	644.5	4.2
145	10 407	3899.8986	2.9	3.500 042 4	1.40	651.9	3.1
152	9607	3600.0692	3.0	3.500 037 7	1.20	665.7	3.2
153	10 407	3899.9130	4.4	3.500 031 9	1.15	650.9	4.6
154	10 941	4099.9928	2.6	3.500 034 1	1.20	658.9	2.8
155	9607	3600.0990	3.8	3.500 029 2	1.10	658.9	4.0

[a] $VC = \frac{1}{2}\langle[\beta_z^2]\rangle \times 10^6$.

[b] $A' = (a' - 0.001\,159) \times 10^9$.

tion of experimental parameters from run to run (e.g., replacement of the polarizing foil, varying adjustment of the compensating gradient, etc.). The maximum systematic variation of $\langle[E_\perp]\rangle$ is therefore estimated to be ± 0.1 mV/cm. This variation in field results in a systematic uncertainty $\sigma_X(a') = 0.35X$ ppm, where X is in units of kG^{-1}.

Experimental Dependence of a' on Electron Beam Current

A series of runs was made to test for a shift in a' as a function of beam current incident on the polarizing foil. At 5.0 MHz, a' was measured with the normal beam current of 4 mA, and with an in-

creased current of 20 mA. The measured shift was -0.05 ± 0.11 ppm/mA. At the current used in the data runs, the interpolated shift in a' is -0.21 ± 0.45 ppm. At 3.5 MHz, the measured shift was 0.54 ± 0.50 ppm/mA. At the 2-mA beam current used in the data runs, the interpolated shift in a' is 1.1 ± 1.0 ppm. These results show no significant shift in a' at a level of 1 ppm, and thus verify the theoretical calculations of the effect of space charge made above. The results also indicate that there is no significant dependence of a' on beam current owing to charging of possible dielectric surface films on the interior of the trapping cylinders.

A similar test was made as a function of pressure. The measured shift of a' with pressure at 4.0 MHz was 0.07 ± 0.8 ppm per 10^{-8} Torr (as indicated on the system ion gauge). Since the gauge pressure for the data runs was less than 10^{-8} Torr, there is no significant pressure dependence.

Statistical Analysis

Although the error estimates $\sigma^*(a_i')$ account for the dependence of a' on all known explicit variables, they may neglect one or more "hidden variables." In particular, a' is an implicit function of $\langle [E_\perp] \rangle$. If $\langle [E_\perp] \rangle$ varies from run to run, the measured values of a_i' will exhibit greater variance than would be expected from *a priori* considerations. In order to detect the systematic effects of a time-varying electric field, we will resort to a simple statistical analysis of a_i'.

The best experimental estimate of a' at each nominal magnetic field is the weighted mean of a_i'. Using weight $w_i^* = \sigma_i^{*-2}$, we have

$$\hat{a}' = \sum_{i=1}^{n} w_i^* a_i' .$$

The caret indicates a quantity evaluated by *a posteriori* analysis of the experimental data. The estimated *a priori* error in $\hat{a}'$ is $\sigma^*(\hat{a}') = (\sum_i w_i^*)^{-1/2}$. The expected and actual dispersion can be compared by calculating $\hat{\chi}^2 = \sum_i (\hat{a}' - a_i')^2 / \sigma_i^{*2}$.[30] The experimental error in $\hat{a}'$ is $\hat{\sigma}(\hat{a}') = \sigma^*(\hat{a}') \{\hat{\chi}^2/(n-1)\}^{1/2}$, where $n-1$ is the number of degrees of freedom. The results at each magnetic field are given in Table III, where $A = (a' - 0.001\,159) \times 10^9$, and P is the probability of $\hat{\chi}^2 \geq \chi^2$ for $n-1$ degrees of freedom. The values of P imply that we can reject the hypothesis that $\hat{\sigma}(\hat{a}') = \sigma^*(\hat{a}')$ at a 95% confidence level for the 5.0-MHz data, and at a 99.5% confidence level for the 3.5-MHz data.

The excessive dispersion of the data can be attributed to (i) an underestimate of $\sigma^*(a_i')$ owing to improper assessment of the error in the explicit variables, or (ii) an additional source of variance owing to the implicit dependence on one or more variables that were not constant from run to run, or (iii) a combination of (i) and (ii). Although there is no statistical justification for the decision, we believe interpretation (ii) to be the most probable. The most likely source of variance is a slow (day to day) drift in the electric field from contact potentials.

We note that several runs differ "suspiciously" from the mean of the averaged data. The large $\hat{\chi}^2$ at 5.0 MHz is due primarily to run 005 (3.0 σ^* below the mean). At 3.5 MHz, runs 125 (2.9 σ^* low), 126 (3.4 σ^* low), and 152 (3.6 σ^* high) are primarily responsible for the high $\hat{\chi}^2$. If Chauvenet's criterion[31] were to be employed, these runs could be rejected, and the dispersion of the remaining data would be statistically acceptable. The *a priori* and *a posteriori* errors would then be in satisfactory agreement. However, in rejecting four runs out of a total of 47, we would be, in effect, ignoring strong statistical evidence that something other than a random statistical fluctuation or apparatus malfunction has occurred. Since we have no basis for deleting these runs because of a suspected apparatus malfunction, we have chosen to retain the four suspicious runs in the final analysis of the data. Accordingly, we will use the experimental error $\hat{\sigma}(\hat{a}')$ as the most probable error in $\hat{a}'$. In using $\hat{\sigma}(\hat{a}')$, we note that the distribution of $\hat{a}'$ at each nominal field is not Gaussian. The quantity $(a' - \hat{a}')/\hat{\sigma}(\hat{a}')$ will be distributed as Student's t for $n-1$ degrees of freedom, where the n observations a_i' are drawn from a Gaussian distribution with mean a'. We will explicitly consider the effects of the non-Gaussian distribution of $\hat{a}'$ in evaluating the confidence intervals for a.

At this point in the analysis, the effect of the ab-

TABLE III. Averaged results of the data runs. See text for an explanation of the tabulated quantities.

Magnetic field (MHz)	A	$\sigma^*(\hat{a}')$ (ppm)	$\hat{\sigma}(\hat{a}')$ (ppm)	$\hat{\chi}^2$	$n-1$	P	$\sigma(\hat{a}')$ (ppm)
5.0	654.25	0.77	1.06	22.0	12	0.04	1.45
4.5	656.85	0.81	0.80	4.9	5	0.4	1.27
4.0	656.70	0.85	0.91	6.8	6	0.3	1.34
3.5	652.48	0.88	1.48	56.0	20	0.005	1.78

solute uncertainty in $\langle[f]\rangle$ must be included. The final uncertainty in $\hat{a}'$ is the rms sum of the 1.0-ppm uncertainty in $\langle[f]\rangle$ and the error $\hat{\sigma}(\hat{a}')$ of the mean. The final error in $\hat{a}'$ is $\sigma(\hat{a}')$, as given in Table III.

E. Evaluation of a

A linear least-squares fit of $\hat{a}'$ vs X (Fig. 11) gives $\hat{a} = (1\,159\,657.7 \pm 3.1) \times 10^{-9} \pm 2.7$ ppm, $\langle[\hat{E}_\perp]\rangle = 0.43 \pm 0.59$ mV/cm, and $\hat{\chi}^2 = 3.58$ for two degrees of freedom. The errors are *a priori* estimates based on the uncertainties of $\hat{a}'(X)$, with the assumption that $\hat{a}'$ is distributed normally. We have considered the effect of the non-normal distribution of $\hat{a}'$ by Monte Carlo methods. The expected confidence intervals[21] for $\hat{a}$ are listed in Table IV. The expected confidence intervals are somewhat larger than those derived from a normal distribution with $\sigma = 2.7$ ppm. The expectation value of χ^2 for two degrees of freedom is 2.9, as compared with the value of 2.0 obtained from a normal distribution. The probability of $\hat{\chi}^2$ exceeding 3.58 is approximately 0.3. The predicted and actual dispersion of the data of $\hat{a}'$ vs X are therefore in satisfactory agreement.

We regard the value of $\hat{\chi}^2$ obtained from the least-squares fit as being a test of the hypothesis that $\hat{a}'$ is a linear function of X. There is no statistical evidence to dispute this hypothesis. The necessity of increasing the error in $\hat{a}'$ from that predicted from *a priori* estimates suggests that a' may have been a function of some additional variable, perhaps a time-varying radial electric field. However, when the experimental error in $\hat{a}'$ is used in the least-squares fit, there is no statistical basis for assuming that the average value of $\langle[E_\perp]\rangle$ was different at the various values of X. This indicates that if there was a radial field present which varied slowly in time, the sequence of taking data at different values of X was sufficiently random to average out the effects of any variation. The hypothesis of a time-invariant field (in the sense of an average

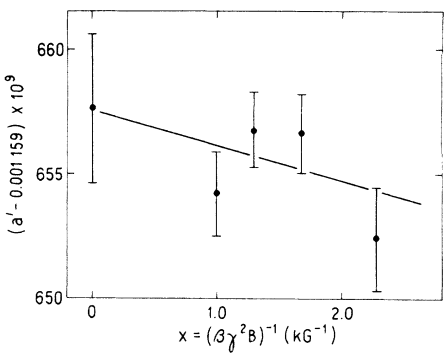

FIG. 11. Extrapolation to determine a.

TABLE IV. Expected confidence intervals for $\hat{a}$.

Confidence level (%)	Interval (ppm)	Interval (ppm) normal distribution, $\sigma = 2.7$ ppm
68	±2.9	±2.7
95	±5.9	±5.2
99.5	±8.7	±7.5

over the entire series of runs) cannot be disproven statistically. Hypothesis (ii) (Sec. IV D) cannot be rejected at a 68% confidence level.

In view of the suspicious nature of runs 005, 125, 126, and 152, we have also evaluated $\hat{a}$ with these runs deleted. This reduces $\hat{a}$ by 0.2 ppm and reduces the error and $\hat{\chi}^2$ by about 10%. None of these changes are statistically significant. Our final result is therefore essentially independent of whether the four suspicious runs are included or deleted.

Confidence Intervals for a

The final error in a is the rms sum of (i) error in $\hat{a}$, (ii) error from systematic dependence of a' on X, (iii) error due to neglecting the quadratic term of Eq. (11), and (iv) additional errors associated with the mapper probe calibration and with field mapping.

The error in $\hat{a}$ is ±2.7 ppm. For a systematic dependence $\sigma_X(a') = 0.35X$ ppm, the systematic error in a after extrapolation is ±0.83 ppm. The systematic error from neglecting the quadratic term in Eq. (11) is less than ±0.2 ppm of a, and is therefore negligible in comparison with the other errors.[21] Several small errors associated with the mapper probe calibration and field mapping are identical for each of the data runs. These errors are (a) uncertainty in Klein's measurement of $\{\omega_p(S)/\omega_0\}$, ±0.5 ppm, (b) uncertainty in ϵ, ±0.2 ppm, (c) uncertainty in $\langle[f]\rangle$ owing to error in z_2^*, ±0.2 ppm, and (d) uncertainty in $\langle[f]\rangle$ from the uncorrected effect of the magnetic properties of the analyzing foil and baffle assembly, ±0.2 ppm. The rms sum of these errors is ±0.7 ppm.

The rms sum of errors (ii)–(iv) is ±1.18 ppm. The final confidence intervals for a are obtained by taking the rms sum of the confidence intervals for this error and the confidence intervals for $\hat{a}$. Since the intervals for $\hat{a}$ depart slightly from those of a normal distribution, the rms sum must be performed individually at each confidence level. The final confidence intervals for a are $\pm 3.5 \times 10^{-9}$ (68% confidence level), $\pm 7.2 \times 10^{-9}$ (95%), and $\pm 10.7 \times 10^{-9}$ (99.5%).

Error Analysis Summary

Because of the complexity of the error analysis necessary in g-IV, it is relatively difficult to trace

TABLE V. Summary of errors.

Source of error	Magnitude (ppm)
Statistical uncertainty in $\{N\langle[\tau_D]\rangle\}$	±2.0
Absolute error in $\langle[f]\rangle$	±1.7
Systematic dependence of a' on X	±1.0
$\omega_p(M)$ to ω_0 conversion	±0.7
Miscellaneous	±1.0
rms sum	±3.0

the contribution of each individual source of error to the final error in a. As an aid to the reader, the major sources of error and their effective rms contribution to the final error in a are given in Table V. The values in this table are accurate to about 10%.

V. RESULTS AND CONCLUSIONS

The final result of g-IV is

$$a_{\text{expt}}(e^-) = (1\,159\,657.7 \pm 3.5)\times 10^{-9} \pm 3.0 \text{ ppm} \quad (25)$$

(68% confidence level). If this result is combined with the currently accepted value of the fine-structure constant[2] ($\alpha^{-1} = 137.036\,08 \pm 0.000\,26$) and the theoretical values for the second- and fourth-order coefficients, the result

$$a_{\text{expt}}(e^-) - [0.5(\alpha/\pi) - 0.328\,48\,(\alpha/\pi)^2] = (1.68 \pm 0.33)\,(\alpha/\pi)^3 \quad (26)$$

can be interpreted as an experimental determination of the sixth-order contribution to the anomaly. The error given in Eq. (26) is the rms sum of the error from g-IV and the error in α^{-1}.

We note that the preliminary result of g-IV was $a = (1\,159\,644 \pm 7)\times 10^{-9}$.[1] This value was obtained from the data of runs 001–015.

The results of g-IV fail to confirm the revised result of g-III (Fig. 12). The difference between the two experiments is

$$a_{g\text{-IV}} - a_{g\text{-III, corrected}} = (109 \pm 30)\times 10^{-9}\,. \quad (27)$$

In order to establish the significance of this discrepancy, further consideration of the g-III confidence intervals for a is necessary. If these intervals are known to be those of a normal distribution, then Eq. (27) implies a discrepancy at the 99.9% confidence level (3.5 standard deviations). If, however, only *a posteriori* statistical methods are used to estimate the error in a' at each nominal magnetic field (as was done in Refs. 14 and 16), the arguments of Sec. IV D should also be applied to g-III. On this basis, we estimate that the 99% confidence interval for g-III would be approximately $\pm 100\times 10^{-9}$, so that Eq. (27) would imply a discrepancy at about the 99% confidence level. Regardless of which statistical interpretation of the data one uses, we feel that the discrepancy with g-IV remains significant. Accordingly, we, in collaboration with G. W. Ford, have subjected the theory and experimental procedures of both experiments to an extensive critical review. No concrete basis for the discrepancy has yet been found.

Comparison with other Experiments

At the present time, no other experimental technique for measuring a has reached sufficient accuracy to check the results of the Michigan $g-2$ experiments. Gräff, Klempt, and Werth[32] have reported a result of $a = (1\,159\,660 \pm 300)\times 10^{-9}$, while Walls[33] has obtained the result $a = (1\,159\,580 \pm 80)\times 10^{-9}$. Both of these experiments use variations of an rf spectroscopic technique to measure ω_c and ω_D directly for thermalized electrons confined in a Penning-configuration ion trap.

Comparison with QED *Theory*

As we have noted in the Introduction, there is currently no complete calculation of the sixth-order coefficient. Our experimental result is somewhat higher than current estimates of the coefficient, but we feel that any speculation on the difference is premature, pending the results of an exact theoretical calculation.

Future Experiments

In view of the role of experimental measurements of a as a test of QED, it is important that additional measurements of a be made at an accuracy of several ppm, using independent techniques. The rf-resonance experiments mentioned above show considerable promise of reaching and perhaps surpassing this level of precision.

With respect to the Michigan $g-2$ technique, any

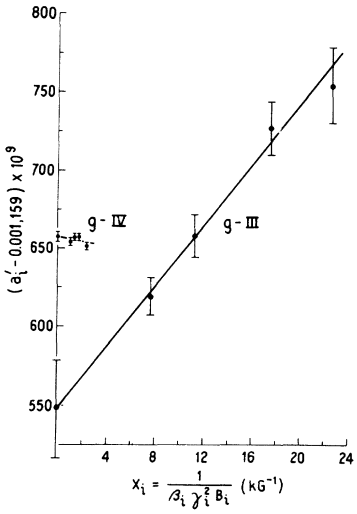

FIG. 12. Comparison of the results of g-III and g-IV.

further increase in precision will be difficult. Some of the problems can be seen from the sources of error given in Table V. The most obvious improvement would be to reduce the statistical timing error. However, a statistical error of ±1 ppm would require running times approaching 1 yr. The uncertainty in the time- and ensemble-average magnetic field can probably be reduced by a factor of 2 through a combination of a shallower trap and more accurate measurement of the density function, but only at the expense of a further reduction in the data rate. The only factor prohibiting a twofold reduction in the systematic error is the running time necessary to complete the required investigations. Therefore, the data rate is the limiting factor. We estimate that a determined effort with the present apparatus (i.e., substantial modifications and 1-yr data runs) might yield at most a factor of 2 increase in accuracy. We feel that such an attempt would not be worth the large investment of time and effort necessary. Accordingly, we have concluded our current electron $g-2$ work.

ACKNOWLEDGMENTS

We wish to thank Professor G. W. Ford for his extensive efforts towards a precise understanding of our experiment, and for many valuable discussions. Professor H. R. Crane has also provided thought provoking critiques of our work. D. Hartman was responsible for the mechanical construction of the apparatus, and G. Edict designed and built much of the electronic circuitry. I. Bigio assisted throughout the construction and testing of the apparatus, as well as during the many months of data taking.

APPENDIX: ERROR ESTIMATE

The errors in the parameters R, δ, and ϕ can be estimated using the method of maximum likelihood. It will be convenient to rewrite Eq. (3) in the form

$$F(A_k, T_i) \equiv F_i \equiv A_1 + A_2\cos(\omega T_i + A_3)\,, \tag{A1}$$

where $k = 1, 2, 3$. The A_k are unknown parameters to be estimated, while ω and T_i are assumed to be exactly known. Suppose that we count with a scaler for a standard observation time in order to measure F at M discrete values of T_i. Let the result of each measurement be N_i and let the residual at the ith point be defined by $r_i \equiv N_i - F_i$. If $\bar{N}_i$ is the mean number of counts observed, and if p is the probability of obtaining one or more counts in a single machine cycle, then in the limit $N_i \gg 1$, the variance in N_i is $\sigma^2(N_i) \equiv \sigma_i^2 = \bar{N}_i(1-p)$.[34]

Since the distribution of N_i is approximately normal, the distribution of r_i will also be normal, with variance σ_i and mean zero. The probability of obtaining a given set of r_i is given by the likelihood function L, defined as

$$L = \prod_{i=1}^{M} [(2\pi)^{1/2}\sigma_i]^{-1} \exp(\tfrac{1}{2}r_i^2/\sigma_i^2). \tag{A2}$$

If we let $W \equiv \ln L$, we have $W \equiv C - \frac{1}{2}q$, where

$$C \equiv \sum_{i=1}^{M} \ln[1/\sigma_i(2\pi)^{1/2}]$$

and

$$q = \sum_{i=1}^{M} (r_i^2/\sigma_i^2)\,.$$

In order to obtain the maximum-likelihood estimates of A_k, denoted by $\hat{A}_k$, it is necessary to maximize $L(\hat{A}_k)$, which is equivalent to minimizing q. Since F is a nonlinear function of A_k, the usual least-squares condition $\partial q/\partial A_k|_{\hat{A}_k}$ is necessary but not sufficient for a minimum in q. In general, an iteration procedure must be used to determine $\hat{A}_k$. In what follows, we will assume that this has been done.

We now wish to estimate the variance in $\hat{A}_k$. To do so, we make use of the fact that the new random variables $a_k \equiv A_k - \hat{A}_k$ will be (to a good approximation) distributed according to

$$L(\vec{a}) \sim \exp\left(-\tfrac{1}{2}\sum_{k,m} H_{km}a_k a_m\right), \tag{A3}$$

where $\vec{a} = (a_1, a_2, a_3)$, and $H_{km} = \partial^2 W/\partial A_k \partial A_m|_{\hat{A}_k}$.[35] The variance-covariance (error) matrix is therefore given by

$$\mathrm{cov}(A_k, A_m) = (H^{-1})_{km}\,, \tag{A4}$$

so that the variance in $\hat{A}_k$ is $\sigma^2(\hat{A}_k) = (H^{-1})_{kk}$.

Before evaluating H, we note that $A_2 \ll A_1$. Therefore, to a sufficient approximation, we can replace σ_i by the constant value $\sigma = [A_1(1-p)]^{1/2}$. After differentiating, we obtain

$$H_{km} = \sigma^{-2}\sum_{i=1}^{M} \frac{\partial F_i}{\partial A_k}\frac{\partial F_i}{\partial A_m} - r_i\frac{\partial^2 F_i}{\partial A_k \partial A_m}\bigg|_{\vec{\hat{A}}_k}\,. \tag{A5}$$

Since, on the average, terms linear in r_i tend to zero, the expectation value of H is

$$\bar{H}_{km} = \sigma^{-2}\sum_{i=1}^{M} \frac{\partial F_i}{\partial A_k}\frac{\partial F_i}{\partial A_m}\bigg|_{\vec{\hat{A}}_k}\,. \tag{A6}$$

Using $\theta_i = \omega T_i$, we find

$$\bar{H}_{11} = \frac{M}{\sigma^2}\,, \qquad \bar{H}_{12} = \frac{1}{\sigma^2}\sum_{i=1}^{M}\cos(\theta_i + A_3)\,, \qquad \bar{H}_{13} = \frac{-A_2}{\sigma^2}\sum_{i=1}^{M}\sin(\theta_i + A_3)\,,$$

$$\bar{H}_{21}=\bar{H}_{12}\,,\qquad \bar{H}_{22}=\frac{1}{\sigma^2}\sum_{i=1}^{M}\cos^2(\theta_i+A_3)\,,\qquad \bar{H}_{23}=\frac{-A_2}{2\sigma^2}\sum_{i=1}^{M}\sin 2(\theta_i+A_3)\,,$$

$$\bar{H}_{31}=\bar{H}_{13}\,,\qquad \bar{H}_{32}=\bar{H}_{23}\,,\qquad \bar{H}_{33}=\frac{A_2^2}{\sigma^2}\sum_{i=1}^{M}\sin^2(\theta_i+A_3)\,. \tag{A7}$$

For arbitrary values of $\Delta\theta=\theta_i-\theta_{i-1}$, the expressions for $\sigma(\hat{A}_k)$ will be rather complex. If, however, we arrange to take data so that $\Delta\theta_i=\frac{1}{2}\pi$ *and* over an integral number of cycles, then all $\bar{H}_{km}$ are zero if $k\neq m$. Since $\bar{H}$ is then diagonal, $\sigma^2(\hat{A}_k)=(\bar{H}_{kk})^{-1}$. Using $N_T=MA_1$ for the total number of counts recorded, and $\sigma=[A_1(1-p)]^{1/2}$, we find

$$\sigma(\hat{A}_1)=[(1-p)N_T]^{1/2}\,, \tag{A8a}$$

$$\sigma(\hat{A}_2)=\hat{A}_1[2(1-p)/N_T]^{1/2}\,, \tag{A8b}$$

$$\sigma(\hat{A}_3)=(\hat{A}_1/\hat{A}_2)[2(1-p)/N_T]^{1/2}\,. \tag{A8c}$$

Although these relations have been derived for $\Delta\theta=\frac{1}{2}\pi$, our experience with the nonlinear estimation program (Sec. IV A) has shown that they are accurate to about 10% for eight points equally spaced over an interval of π or greater. If $\hat{A}_1$, $\hat{A}_2$, and $\hat{A}_3$ are replaced by R_0^K, $R_0^K\delta_K$, and ϕ_K, and if p is neglected ($p\leq 0.05$ in g-IV), one obtains Eqs. (23a)–(23c).

*Work supported by the U. S. Atomic Energy Commission.

†Present address: Gibbs Laboratory, Yale University, New Haven, Conn. 06520.

[1]J. C. Wesley and A. Rich, Phys. Rev. Letters 24, 1320 (1970).

[2]B. N. Taylor, W. H. Parker, and D. N. Langenberg, Rev. Mod. Phys. 41, 375 (1969).

[3]R. P. Feynman, *Quantum Electrodynamics* (Benjamin, New York, 1961).

[4]J. Schwinger, Phys. Rev. 73, 416 (1948); 74, 1439 (1948); 75, 651 (1949); 76, 790 (1949).

[5]A. Petermann, Nucl. Phys. 5, 677 (1958).

[6]C. M. Sommerfield, Phys. Rev. 107, 328 (1958); Ann. Phys. (N.Y.) 5, 26 (1958).

[7]The original calculation of B by R. Karplus and N. M. Kroll [Phys. Rev. 77, 536 (1950)] was later found to be incorrect.

[8]S. D. Drell and H. R. Pagels, Phys. Rev. 140, B397 (1965).

[9]R. G. Parsons, Phys. Rev. 168, 1562 (1968).

[10]J. A. Mignaco and E. Remiddi, Nuovo Cimento 60A, 519 (1969).

[11]J. Aldins, T. Kinoshita, S. J. Brodsky, and A. Dufner, Phys. Rev. Letters 23, 441 (1969); Phys. Rev. D 1, 2378 (1970).

[12]S. J. Brodsky and T. Kinoshita, in *Proceedings of the Fifteenth International Conference on High-Energy Physics, Kiev*, 1970 (Academy of Sciences, U.S.S.R., Moscow, 1970).

[13]M. J. Levine and J. Wright, Carnegie-Mellon University and University of Illinois report, 1970 (unpublished).

[13a]M. J. Levine and J. Wright, Phys. Rev. Letters 26, 1351 (1971).

[14]D. T. Wilkinson and H. R. Crane, Phys. Rev. 130, 852 (1963).

[15]J. W. M. DuMond and E. R. Cohen, Phys. Rev. Letters 1, 291 (1958).

[16]A. Rich, Phys. Rev. Letters 20, 967 (1968); 21, 1221(E) (1968).

[17]F. J. M. Farley, in *Cargese Lectures in Physics*, edited by M. Lévy (Gordon and Breach, New York, 1968), Vol. 2.

[18]G. R. Henry and J. E. Silver, Phys. Rev. 180, 1262 (1969). The correction was also obtained by Ford and Rich in 1969 using an alternative formulation (see Sec. II B).

[19]T. G. Northrup, *The Adiabatic Motion of Charged Particles* (Wiley, New York, 1963), Chap. 3. See also Ref. 20.

[20]J. R. Gilleland, Ph.D. thesis (University of Michigan, 1969), Appendix III (unpublished).

[21]J. C. Wesley, Ph.D. thesis (University of Michigan, 1970) (unpublished).

[22]The observable quantity in g-IV is actually the electron polarization $\vec{P}$, which is proportional to the quantum-mechanical expectation value of $\vec{S}$, i.e., $\langle\vec{S}\rangle$. A quantum-mechanical solution for the motion of $\langle\vec{S}\rangle$ is identical to that obtained classically for a body with angular momentum $\vec{S}$ and $\vec{\mu}=g/2(e/m_0c)\,\vec{S}$. The notation $\langle\ \rangle$ will later be used to denote an average over an ensemble of electrons. This use should not be confused with the quantum-mechanical expectation value.

[23]G. W. Ford and C. W. Hirt, University of Michigan report, contract No. NONR 1224(15), 1961 (unpublished). This problem has also been treated by V. Bargman, L. Michel, and V. L. Telegdi, Phys. Rev. Letters 2, 435 (1959); and by M. Fierz and V. L. Telegdi, in *Quanta*, edited by P. G. O. Freund, C. J. Goebel, and Y. Nambu (Chicago U. P., Chicago, 1970), p. 209.

[24]G. W. Ford (private communication).

[25]G. W. Ford (private communication).

[26]G. W. Ford and S. Granger (private communication).

[27]E. Klein, Z. Physik 208, 28 (1968).

[28]A value of μ_p'/μ_B obtained from a measurement of $g_j(H)/g_p(H_2O)$ reported by E. B. D. Lambe [Ph.D. thesis (Princeton, 1959) (unpublished)] can be used. See A. Rich, in *Proceedings of the Third International Conference on Atomic Masses and Related Constants*, edited by R. Barber (Manitoba U. P., Winnipeg, 1968).

[29]J. C. Wesley and A. Rich, in *Proceedings of the International Conference on Precision Measurement and Fundamental Constants*, Natl. Bur. Std. (U.S.) (U.S. GPO, Washington, D.C., 1971). See N. F. Ramsey, Phys. Rev. A 1, 1320 (1970) for a theoretical discussion of the nonlinearity.

[30]W. C. Hamilton, *Statistics in Physical Science* (Ronald, New York, 1964), Chap. 5.

[31]L. G. Parratt, *Probability and Experimental Errors in Science* (Wiley, New York, 1961), p. 176.
[32]G. Gräff, E. Klempt, and G. Werth, Z. Physik 222, 201 (1969).
[33]F. Walls, Ph.D. thesis (University of Washington, 1970) (unpublished).
[34]A. M. Mood, *Introduction to the Theory of Statistics* (McGraw-Hill, New York, 1950), Sec. 7.7.
[35]J. Orear, Lawrence Radiation Laboratory Report No. UCRL-8417, 1958 (unpublished).

PHYSICAL REVIEW A VOLUME 4, NUMBER 4 OCTOBER 1971

Moment Analysis of Atomic Spectral Lines*

Harry C. Jacobson
Department of Physics and Astronomy, University of Tennessee, Knoxville, Tennessee 37916
(Received 9 April 1971)

The moments of a spectral line are evaluated in a general way and compared with results which invoke standard assumptions of line-broadening theory. Cesium–rare-gas systems are analyzed for a variety of experimental conditions in the hope of extracting useful information about excited-state interactions. The computation uses atomic-beam results for the ground-state interaction and assumes that the excited-state potentials are represented to a first approximation by $V_f = G/R^{12} - D/R^6$. The calculation, which includes a comparison of line shapes, indicates that the following numbers (in cgs units) are reliable for the long-wavelength component of the resonance lines of cesium: with argon, $G = 4.87 \times 10^{-102}$, $D = 4.74 \times 10^{-58}$; with helium, $G = 0.459 \times 10^{-102}$ and $D = -0.614 \times 10^{-58}$. Analysis of the cesium-xenon system yields results which illuminate the practical difficulties associated with an otherwise attractive technique.

I. INTRODUCTION

Realistic calculations of spectral line shapes of gases is a matter of importance in a variety of situations. Significant progress has been made in the case of plasmas, but relatively little has been achieved for the case of (charge) neutral perturbers. The most general formulations of the theory are appropriate for comparison with experiments in which the impact approximation[1] is warranted. Another class of experiments can be analyzed correctly using theories which make the adiabatic approximation.[2] However, in many cases, especially those in which interesting information about excited-state interactions is available, the computation of line shapes with existing theories cannot be justified. The fact that improvements in the theory are difficult to achieve suggests that something simpler than the line shape itself be studied.

The moments of a spectral distribution have been considered profitably in a number of contexts.[3] For example, they have been evaluated for the absorption of light by atoms[4] and molecules[5]; they have been used to establish error bounds on forces between atoms,[6] and to study the potentials involved in collision induced absorption.[7] Moments have been used in line-shape theories,[8] and to infer intermolecular-force information from experiment.[9]

The use of moments to infer information about interactions and to calculate line shapes is an attractive prospect. Using p moments, it would be possible, in principle, to obtain p parameters in a realistic model of an excited-state potential. Moreover, since the line shape is the Fourier transform of a correlation function $C(t)$ and since C can be viewed as a power-series expansion in t with coefficients proportional to the moments, a knowledge of the moments would then permit an accurate determination of C for small times.

These prospects raise several significant questions. What is the general quantum-mechanical form for the first few moments, and how is it simplified when various commonly employed approximations are introduced? Is it possible to infer reliable information about interactions from the moments and if so, how much? The present paper seeks an answer to these questions. Specifically, the first three moments are calculated using an adiabatic representation.[10] These results for the diabatic case are then compared with that obtained by making the adiabatic approximation, the quasistatic approximation,[2] and the approximations used by Fox and Jacobson.[11] Then the problem is restricted to a detailed analysis of data on a cesium resonance line when the cesium is pressurized by helium, argon, and xenon.[12,13] The reliability of the results, which differs in each case, is discussed at the appropriate point and summarized in the conclusions.

II. CALCULATION OF MOMENTS

A. Diabatic

The spectral density $F(\omega)$ for a line-shape prob-